

# Relativistic Hartree-Bogoliubov model with density-dependent meson-nucleon couplings

T. Nikšić and D. Vretenar

*Physics Department, Faculty of Science,  
University of Zagreb, 10 000 Zagreb, Croatia*

P. Finelli

*Physics Department, University of Bologna,  
and INFN - Bologna, I-40126 Bologna, Italy*

P. Ring

*Physik-Department der Technischen Universität München, D-85748 Garching, Germany*

(Dated: October 25, 2018)

## Abstract

The relativistic Hartree-Bogoliubov (RHB) model is extended to include density dependent meson-nucleon couplings. The effective Lagrangian is characterized by a phenomenological density dependence for the  $\sigma$ ,  $\omega$  and  $\rho$  meson-nucleon vertex functions, adjusted to properties of nuclear matter and finite nuclei. Pairing correlations are described by the pairing part of the finite range Gogny interaction. The new density-dependent effective interaction DD-ME1 is tested in the analysis of the equations of state for symmetric and asymmetric nuclear matter, and of ground-state properties of the Sn and Pb isotopic chains. Results of self-consistent RHB calculations are compared with experimental data, and with results previously obtained in the RHB model with non-linear self-interactions, as well as in the density dependent relativistic hadron field (DDRH) model. Parity-violating elastic electron scattering on Pb and Sn nuclei is calculated using a relativistic optical model with inclusion of Coulomb distortion effects, and the resulting asymmetry parameters are related to the neutron ground-state density distributions.

PACS numbers: 21.60.-n, 21.30.Fe, 21.65.+f, 21.10.-k

## I. INTRODUCTION

Models based on concepts of nonrenormalizable effective relativistic field theories and density functional theory provide a rich theoretical framework for studies of nuclear structure phenomena, not only in nuclei along the valley of  $\beta$ -stability, but also in exotic nuclei with extreme isospin values and close to the particle drip lines. A well known example of an effective theory of nuclear structure is Quantum Hadrodynamics (QHD), a field theoretical framework of Lorentz-covariant, meson-nucleon or point-coupling models of nuclear dynamics [1]. The effective Lagrangians of QHD consist of known long-range interactions constrained by symmetries and a complete set of generic short-range interactions. The QHD framework implicitly includes vacuum effects, chiral symmetry, nucleon substructure, exchange terms, long- and short-range correlation effects.

Structure models based on the relativistic mean-field (RMF) approximation have been successfully employed in studies of spherical and deformed nuclei all over the periodic table [2]. The relativistic framework has also been applied in studies of nuclear structure phenomena in nuclei far from  $\beta$ - stability. In particular, in studies of isotopic chains that also included exotic nuclei with extreme isospin values, we have used the relativistic Hartree-Bogoliubov (RHB) model, which encloses a unified description of mean-field and pairing correlations. A number of interesting nuclear properties have been studied with the RHB model: the halo phenomenon in light nuclei [3], properties of light neutron-rich nuclei [4], the reduction of the effective single-nucleon spin-orbit potential in nuclei close to the drip-lines [5], properties of neutron-rich Ni and Sn isotopes [6], the location of the proton drip-line between from  $Z = 31$  to  $Z = 73$  and the phenomenon of ground-state proton radioactivity [7, 8, 9].

The details of calculated nuclear properties that can be compared with empirical data, as well as the predictions of new phenomena far from  $\beta$ -stability (halo nuclei, neutron skins, suppression of shell effects in neutron rich nuclei, ground-state proton radioactivity beyond the drip-line, the onset of exotic collective modes), crucially depend on the choice of the effective RMF Lagrangian in the  $ph$  channel, as well as on the treatment of pairing correlations. Several phenomenological parameterizations of the effective Lagrangian have been derived that provide a satisfactory description of nuclear properties along the  $\beta$ -stability line, as well as in regions far from stability. These effective interactions are characterized by a

minimal set of model parameters: meson masses and meson-nucleon coupling constants. The most successful RMF effective interactions are purely phenomenological, with parameters adjusted to reproduce the nuclear matter equation of state and a set of global properties of spherical closed-shell nuclei. In most applications of the RHB model, in particular, we have used the NL3 effective interaction [10] for the RMF effective Lagrangian. Properties calculated with NL3 indicate that this is probably the best effective interaction so far, both for nuclei at and away from the line of  $\beta$ -stability.

The limitations of standard RMF effective interactions are, however, well known, even for nuclei close to the stability line. They are more pronounced in the isovector channel, which is poorly constrained by the available experimental data on ground-state properties of nuclei. For example, in a recent analysis of neutron radii in the framework of mean-field models [11], it has been shown that conventional RMF models systematically overestimate the values of  $r_n - r_p$ . It is well known that they also predict an equation of state of neutron matter that is very different from the standard microscopic many-body neutron matter equation of state of Friedman and Pandharipande [12]. The parameterization of the isovector channel of an effective RMF interaction is, of course, extremely important for possible extrapolations to neutron-rich or proton-rich nuclei. For example, various non-relativistic and relativistic mean-field models differ significantly in the prediction of the two-neutron separation energies of the Sn isotopes with  $A > 132$  [13] and, therefore, of the exact location of the drip-line. There are also differences in the predicted location of the drip-line on the proton-rich side [9]. The properties of effective interactions are very important for the description of phenomena in nuclear astrophysics. The choice of the effective RMF Lagrangian directly determines the calculated properties of neutron stars (radii, surface crust) [14, 15], as well as the properties of nuclei that take part in the r-process or rp-process of nucleosynthesis.

In order to overcome the limitations of standard RMF models, several solutions have been put forward. An obvious choice is to extend the minimal six-parameter RMF model by including additional interaction terms in the isoscalar, as well as in the isovector channel. The complex many-body dynamics is effectively included in additional non-linear self-interactions. This approach has been studied both in the framework of meson-exchange models [15, 16, 17, 18] and with relativistic point-coupling models [19, 20]. Even though some interesting results have been obtained, especially in applications to nuclear astrophysics, the situation is not satisfactory. The problem is that the empirical data set of bulk

and single-particle properties of finite nuclei can only constrain six or seven parameters in the general expansion of an effective Lagrangian [21]. One can, of course, include interaction terms that describe specific phenomena, but their coupling parameters and even their forms cannot be accurately determined in this way. In some cases even the signs of interaction terms are not determined by the data. The general expansion of an effective Lagrangian in powers of the fields and their derivatives can be controlled by the “naive dimensional analysis” (NDA) [19, 20, 22, 23]. NDA tests the coefficients of the expansion for “naturalness”, i.e. this method controls the magnitude of the coupling constants. Although NDA can exclude some interaction terms because their couplings would be “unnatural”, it cannot determine the parameters of a model on a level of accuracy that is required for a quantitative analysis of nuclear structure data.

Instead of including additional non-linear self-interaction terms in effective RMF Lagrangians, another possibility is to formulate an effective hadron field theory with medium dependent meson-nucleon vertices. Such an approach retains the basic structure of QHD, but could be more directly related to the underlying microscopic description of nuclear interactions. In the density dependent relativistic hadron field (DDRH) model of Refs. [24, 25, 26] the medium dependence of the vertices is expressed by a functional of the baryon field operators. The meson-baryon coupling constants in nuclear matter are adjusted to the Dirac-Brueckner (DB) self-energies. A Lorentz-invariant functional is defined to project the nuclear matter results onto the meson-nucleon vertices of the effective DDRH model for finite nuclei. In the early version [24] of this model, the density dependence was only included in the field equations after the variation. However, a consistent treatment of medium effects implies a variation of the vertex functionals with respect to the baryon field operators, and this results in additional rearrangement self-energies in the single-nucleon Dirac equation [26]. In Ref. [26] the model was applied in the calculation of ground-state properties of doubly-closed shell nuclei. Density dependent  $\sigma$  and  $\omega$  meson couplings were used that were derived from DB calculations using the Bonn A, B, and C nucleon-nucleon potentials. It was shown that the inclusion of rearrangement self-energies is essential for a quantitative description of bulk properties and single-particle spectra. The model has been recently extended to hypernuclei [27], neutron star matter [28], and asymmetric nuclear matter and exotic nuclei [29]. The density dependent interactions have been derived from the Groningen and Bonn-A nucleon-nucleon potentials. For finite nuclei, in particular, the quality of the

calculated properties are comparable with non-linear RMF models.

In Ref. [30] Typel and Wolter introduced a phenomenological density dependence for the  $\sigma$ ,  $\omega$  and  $\rho$  meson-nucleon couplings, adjusted to properties of nuclear matter and some finite nuclei. The parameters of their DDRH model were also compared with coupling constants derived from DB calculations of nucleon self-energies. The model was used to study the equation of state of symmetric and asymmetric nuclear matter, and the ground state properties of semi-closed shell nuclei. Even though pairing correlations were only treated in the BCS approximation, properties at the proton and neutron drip-lines were calculated. It was, however, emphasized that a more realistic description of nuclei at the drip-lines necessitates the use of the Hartree-Bogoliubov framework with finite range pairing interactions. The phenomenological ansatz of Ref. [30] for the functional form of the density dependence of the meson-nucleon vertices was also used in Ref. [29] to derive the meson-nucleon coupling parameters from the Groningen and Bonn-A NN potentials.

In this work we present an extension of the relativistic Hartree-Bogoliubov (RHB) model that includes density dependent meson-nucleon couplings. For the effective RMF Lagrangian we follow the approach of Typel and Wolter [30] and use their phenomenological functional forms for the density dependence of the vertex functions. The parameters of the effective interaction are, however, adjusted in a different way. Pairing correlations are described by the pairing part of the finite range Gogny interaction. The new model is tested in the analysis of the equation of state for symmetric and asymmetric nuclear matter, and ground-state properties of the Sn and Pb isotopic chains. The results are compared with experimental data and with previous results obtained in the RHB, as well as DDRH frameworks.

In Sec. II we outline the RHB model with density dependent meson-nucleon couplings. The new parameterization of the vector density dependence of the vertex functionals is discussed in Sec. III in comparison with the effective interaction of Typel and Wolter, and we also analyze the results for the equation of state for symmetric and asymmetric nuclear matter. In Sec. IV the new density-dependent effective interaction DD-ME1 is employed in the RHB calculations of ground-state properties of Sn and Pb nuclei. Binding energies, charge radii, differences between neutron and proton radii, spin-orbit splittings, and charge isotope shifts are compared with available experimental data, and with the results obtained with the non-linear interaction NL3. Sec. V contains an analysis of parity-violating elastic electron scattering on  $^{208}\text{Pb}$  and on those Sn isotopes for which there are experimental data

on  $r_n - r_p$ . For the elastic scattering of 850 MeV electrons on these nuclei, the calculated parity-violating asymmetry parameters are related to the Fourier transforms of the neutron density distributions. In Sec. VI we summarize the results of this work and present an outlook for future applications of the RHB model with density-dependent meson-nucleon couplings.

## II. RELATIVISTIC HARTREE-BOGOLIUBOV MODEL WITH DENSITY-DEPENDENT MESON-NUCLEON COUPLINGS

The framework of density-dependent hadron field theory is described in great detail in Refs. [26, 29, 30]. In this section we outline the essential features of the model with vector density dependence of the meson-nucleon couplings. The model is defined by the relativistic Lagrangian density

$$\begin{aligned} \mathcal{L} = & \bar{\psi} (i\boldsymbol{\gamma} \cdot \boldsymbol{\partial} - m) \psi + \frac{1}{2}(\partial\sigma)^2 - \frac{1}{2}m_\sigma\sigma^2 \\ & - \frac{1}{4}\Omega_{\mu\nu}\Omega^{\mu\nu} + \frac{1}{2}m_\omega^2\omega^2 - \frac{1}{4}\vec{R}_{\mu\nu}\vec{R}^{\mu\nu} + \frac{1}{2}m_\rho^2\vec{\rho}^2 - \frac{1}{4}F_{\mu\nu}F^{\mu\nu} \\ & - g_\sigma\bar{\psi}\sigma\psi - g_\omega\bar{\psi}\boldsymbol{\gamma} \cdot \boldsymbol{\omega}\psi - g_\rho\bar{\psi}\boldsymbol{\gamma} \cdot \vec{\rho}\vec{\boldsymbol{\tau}}\psi - e\bar{\psi}\boldsymbol{\gamma} \cdot \boldsymbol{A}\frac{(1-\tau_3)}{2}\psi. \end{aligned} \quad (1)$$

Vectors in isospin space are denoted by arrows, and bold-faced symbols will indicate vectors in ordinary three-dimensional space. The Dirac spinor  $\psi$  denotes the nucleon with mass  $m$ .  $m_\sigma$ ,  $m_\omega$ , and  $m_\rho$  are the masses of the  $\sigma$ -meson, the  $\omega$ -meson, and the  $\rho$ -meson.  $g_\sigma$ ,  $g_\omega$ , and  $g_\rho$  are the corresponding coupling constants for the mesons to the nucleon.  $e^2/4\pi = 1/137.036$ . The coupling constants and unknown meson masses are parameters, adjusted to reproduce nuclear matter properties and ground-state properties of finite nuclei.  $\Omega^{\mu\nu}$ ,  $\vec{R}^{\mu\nu}$ , and  $F^{\mu\nu}$  are the field tensors of the vector fields  $\omega$ ,  $\rho$ , and of the photon:

$$\Omega^{\mu\nu} = \partial^\mu\omega^\nu - \partial^\nu\omega^\mu \quad (2)$$

$$\vec{R}^{\mu\nu} = \partial^\mu\vec{\rho}^\nu - \partial^\nu\vec{\rho}^\mu \quad (3)$$

$$F^{\mu\nu} = \partial^\mu A^\nu - \partial^\nu A^\mu. \quad (4)$$

$g_\sigma$ ,  $g_\omega$ , and  $g_\rho$  are assumed to be vertex functions of Lorentz-scalar bilinear forms of the nucleon operators. In most applications of the density-dependent hadron field theory the meson-nucleon couplings are functions of the vector density

$$\rho_v = \sqrt{j_\mu j^\mu}, \quad \text{with} \quad j_\mu = \bar{\psi}\boldsymbol{\gamma}_\mu\psi. \quad (5)$$

Another obvious choice is the dependence on the scalar density  $\rho_s = \bar{\psi}\psi$ . It has been shown, however, that the vector density dependence produces better results for finite nuclei [26], and provides a more natural relation between the self-energies of the density-dependent hadron field theory and the Dirac-Brueckner microscopic self-energies [29]. In the following we assume the vector density dependence of the meson-nucleon couplings. The single-nucleon Dirac equation is derived by variation of the Lagrangian (1) with respect to  $\bar{\psi}$

$$[\gamma^\mu(i\partial_\mu - \Sigma_\mu) - (m - \Sigma)]\psi = 0, \quad (6)$$

with the nucleon self-energies defined by the following relations

$$\Sigma = g_\sigma\sigma \quad (7)$$

$$\Sigma_\mu = g_\omega\omega_\mu + g_\rho\vec{\tau} \cdot \vec{\rho}_\mu + e\frac{(1 - \tau_3)}{2}A_\mu + \Sigma_\mu^R. \quad (8)$$

The density dependence of the vertex functions  $g_\sigma$ ,  $g_\omega$ , and  $g_\rho$  produces the *rearrangement* contribution  $\Sigma_\mu^R$  to the vector self-energy

$$\Sigma_\mu^R = \frac{j_\mu}{\rho_v} \left( \frac{\partial g_\omega}{\partial \rho_v} \bar{\psi}\gamma^\nu\psi\omega_\nu + \frac{\partial g_\rho}{\partial \rho_v} \bar{\psi}\gamma^\nu\vec{\tau}\psi \cdot \vec{\rho}_\nu + \frac{\partial g_\sigma}{\partial \rho_v} \bar{\psi}\psi\sigma \right). \quad (9)$$

The inclusion of the rearrangement self-energies is essential for the energy-momentum conservation and the thermodynamical consistency of the model [26, 30].

The lowest order of the quantum field theory is the *mean-field* approximation: the meson field operators are replaced by their expectation values. The  $A$  nucleons, described by a Slater determinant  $|\Phi\rangle$  of single-particle spinors  $\psi_i$ , ( $i = 1, 2, \dots, A$ ), move independently in the classical meson fields. The sources of the meson fields are defined by the nucleon densities and currents. The ground state of a nucleus is described by the stationary self-consistent solution of the coupled system of Dirac and Klein-Gordon equations. Due to charge conservation, only the 3-component of the isovector rho meson contributes. For an even-even system the spatial vector components  $\boldsymbol{\omega}$ ,  $\boldsymbol{\rho}_3$  and  $\mathbf{A}$  vanish, and the self-energies are determined by the solutions of the Klein-Gordon and Poisson equations

$$(-\Delta + m_\sigma)\sigma(\mathbf{r}) = -g_\sigma\rho_s(\mathbf{r}), \quad (10)$$

$$(-\Delta + m_\omega)\omega(\mathbf{r}) = g_\omega\rho_v(\mathbf{r}), \quad (11)$$

$$(-\Delta + m_\rho)\rho_3(\mathbf{r}) = g_\rho(\rho_n(\mathbf{r}) - \rho_p(\mathbf{r})), \quad (12)$$

$$-\Delta A_0(\mathbf{r}) = e^2\rho_c(\mathbf{r}). \quad (13)$$

The source terms on the left-hand side of these equations are sums of bilinear products of baryon amplitudes. The densities are calculated in the *no-sea* approximation, i.e. only occupied single-nucleon states with positive energy explicitly contribute to the nucleon self-energies.

In addition to the self-consistent mean-field potential, pairing correlations have to be included in order to describe ground-state properties of open-shell nuclei. For spherical and deformed nuclei not too far from the stability line, pairing is often treated phenomenologically in the simple BCS approximation [2]. However, the BCS model presents only a poor approximation for exotic nuclei far from the valley of  $\beta$ -stability. The structure of weakly bound nuclei necessitates a unified and self-consistent treatment of mean-field and pairing correlations. In particular, the relativistic Hartree-Bogoliubov (RHB) model [3, 4, 6, 8] represents a relativistic extension of the Hartree-Fock-Bogoliubov (HFB) framework. In the RHB model the ground state of a nucleus  $|\Phi\rangle$  is represented by the product of independent single-quasiparticle states. These states are eigenvectors of the generalized single-nucleon Hamiltonian that contains two average potentials: the self-consistent mean-field  $\hat{\Gamma}$ , which encloses all the long range particle-hole ( $ph$ ) correlations, and a pairing field  $\hat{\Delta}$ , which sums up the particle-particle ( $pp$ ) correlations. In the Hartree approximation for the self-consistent mean field, the relativistic Hartree-Bogoliubov equations read

$$\begin{pmatrix} \hat{h}_D - m - \lambda & \hat{\Delta} \\ -\hat{\Delta}^* & -\hat{h}_D + m + \lambda \end{pmatrix} \begin{pmatrix} U_k(\mathbf{r}) \\ V_k(\mathbf{r}) \end{pmatrix} = E_k \begin{pmatrix} U_k(\mathbf{r}) \\ V_k(\mathbf{r}) \end{pmatrix} \quad (14)$$

where  $\hat{h}_D$  is the single-nucleon Dirac Hamiltonian, and  $m$  is the nucleon mass. The chemical potential  $\lambda$  has to be determined by the particle number subsidiary condition, in order that the expectation value of the particle number operator in the ground state equals the number of nucleons. The column vectors denote the quasiparticle wave functions, and  $E_k$  are the quasiparticle energies. The source terms in equations (10) to (13) are sums of bilinear products of baryon amplitudes

$$\rho_s(\mathbf{r}) = \sum_{E_k > 0} V_k^\dagger(\mathbf{r}) \gamma^0 V_k(\mathbf{r}), \quad (15)$$

$$\rho_v(\mathbf{r}) = \sum_{E_k > 0} V_k^\dagger(\mathbf{r}) V_k(\mathbf{r}), \quad (16)$$

$$\rho_n(\mathbf{r}) - \rho_p(\mathbf{r}) = \sum_{E_k > 0} V_k^\dagger(\mathbf{r}) \tau_3 V_k(\mathbf{r}), \quad (17)$$



$$\rho_c(\mathbf{r}) = \sum_{E_k > 0} V_k^\dagger(\mathbf{r}) \frac{1 - \tau_3}{2} V_k(\mathbf{r}), \quad (18)$$

where the sums run over all positive energy states. In most applications of the RHB model a phenomenological pairing interaction has been used, the pairing part of the Gogny force,

$$V^{pp}(1, 2) = \sum_{i=1,2} e^{-((\mathbf{r}_1 - \mathbf{r}_2)/\mu_i)^2} (W_i + B_i P^\sigma - H_i P^\tau - M_i P^\sigma P^\tau), \quad (19)$$

with the set D1S [31] for the parameters  $\mu_i$ ,  $W_i$ ,  $B_i$ ,  $H_i$ , and  $M_i$  ( $i = 1, 2$ ).

The RHB equations are solved self-consistently, with potentials determined in the mean-field approximation from solutions of Klein-Gordon equations for the meson fields. The Dirac-Hartree-Bogoliubov equations and the equations for the meson fields are solved by expanding the nucleon spinors  $U_k(\mathbf{r})$  and  $V_k(\mathbf{r})$ , and the meson fields in terms of the eigenfunctions of a spherical or deformed axially symmetric oscillator potential. A detailed description of the relativistic Hartree-Bogoliubov model for spherical and deformed nuclei can be found in Refs. [4] and [8], respectively.

### III. PARAMETERIZATION OF THE DENSITY DEPENDENCE OF THE MESON-NUCLEON COUPLINGS

The density dependence of the meson-nucleon couplings can be obtained from microscopic Dirac-Brueckner (DB) calculations of nucleon-self energies in symmetric and asymmetric nuclear matter [26, 32]. However, depending on the choice of the nucleon-nucleon potential and on the approximations in the DB calculation, rather different results are obtained for the density dependence of the vertex functions. At low densities, in particular, DB calculations of nuclear matter become unreliable, and meson-nucleon couplings determined directly from DB self-energies provide only a qualitative description of ground-state properties for finite nuclei. Instead of adjusting the vertex functions directly to DB self-energies, in Ref. [30] an ansatz was made for the functional form of the density dependence that encloses different DB results. The parameters of the density dependence were obtained from a fit to properties of nuclear matter and finite nuclei. The same functional form was also used in Ref. [29] to adjust the meson-nucleon couplings to the DB self-energies derived from the Groningen and Bonn-A nucleon-nucleon potentials. In this work we adopt for the density dependence of the meson-nucleon couplings the functionals of Ref. [30], and adjust the parameters to

properties of symmetric and asymmetric nuclear matter, binding energies, charge radii and neutron radii of spherical nuclei. The coupling of the  $\sigma$ -meson and  $\omega$ -meson to the nucleon field reads

$$g_i(\rho) = g_i(\rho_{\text{sat}})f_i(x) \quad \text{for } i = \sigma, \omega, \quad (20)$$

where

$$f_i(x) = a_i \frac{1 + b_i(x + d_i)^2}{1 + c_i(x + d_i)^2} \quad (21)$$

is a function of  $x = \rho/\rho_{\text{sat}}$ . The eight real parameters in (21) are not independent. The five constraints  $f_i(1) = 1$ ,  $f'_\sigma(1) = f'_\omega(1)$ , and  $f''_i(0) = 0$ , reduce the number of independent parameters to three. Two additional parameters in the isoscalar channel are  $g_\sigma(\rho_{\text{sat}})$  and  $g_\omega(\rho_{\text{sat}})$ . The functional form of the density dependence of the  $\rho$ -meson coupling is suggested by DB calculations of asymmetric nuclear matter [32]

$$g_\rho(\rho) = g_\rho(\rho_{\text{sat}}) \exp[-a_\rho(x - 1)] . \quad (22)$$

The isovector channel is parameterized by  $g_\rho(\rho_{\text{sat}})$  and  $a_\rho$ .

In Ref. [30] the standard free values for the masses of the  $\omega$  and  $\rho$  mesons were taken:  $m_\omega = 783$  MeV and  $m_\rho = 763$  MeV. The mass of the  $\sigma$  meson was fixed to  $m_\sigma = 550$  MeV, and the remaining seven independent parameters were adjusted to nuclear matter properties (three parameters) and to the binding energies of symmetric and neutron-rich nuclei (four parameters). In this work the density-dependent meson-nucleon couplings have been determined using a somewhat different procedure. The parameters have been adjusted simultaneously to properties of nuclear matter (see Table I), and to binding energies, charge radii and differences between neutron and proton radii of spherical nuclei (see Table III). In addition to the seven coupling parameters, the mass of the  $\sigma$ -meson has also been included in the fitting procedure, i.e. we have used one more free parameter with respect to the model of Ref. [30]. For the open shell nuclei in Table III, pairing correlations have been treated in the BCS approximation with empirical pairing gaps (five-point formula). For nuclear matter the "empirical" input was:  $E/A = -16$  MeV (5%),  $\rho_0 = 0.153$  fm $^{-3}$  (10%),  $K_0 = 250$  MeV (10%), and  $J = 33$  MeV (10%). The values in parentheses correspond to the error bars used in the fitting procedure. The binding energies of finite nuclei and the charge radii were taken within an accuracy of 0.1% and 0.2%, respectively. Due to large experimental uncertainties, however, the error bar used for the neutron skin was 5%. After

the solution of the self-consistent equations, we subtract from the total binding energy the microscopic estimate for the center-of-mass correction

$$E_{cm} = -\frac{\langle P_{cm}^2 \rangle}{2Am}, \quad (23)$$

where  $P_{cm}$  is the total momentum of a nucleus with  $A$  nucleons. The resulting parameters of the density-dependent meson-exchange effective interaction (DD-ME1) are displayed in Table I, in comparison to those of Ref. [30] (TW-99). We note two additional differences between these models. In the relativistic mean-field model of Ref. [30] the center-of-mass correction (23) is calculated by using the non-relativistic approximation for the nucleon wave functions, and the Coulomb energy is corrected by multiplying the vector self-energy of the proton with the factor  $(Z - 1)/Z$ . In Table I we first note that, even though  $m_\sigma$  is a free parameter in our model, the adjustment to nuclear matter and to properties of finite spherical nuclei produces a value that is very close to that of the TW-99 parameterization. The two effective interactions display similar values for the meson-nucleon coupling parameters at saturation density  $g_i(\rho_{\text{sat}})$  ( $i = \sigma, \omega, \rho$ ), as well as the value of the parameter  $a_\rho$ , which determines the density-dependence of the  $\rho$ -meson coupling (22). The eight parameters, which characterize the density dependence (21) of the  $\sigma$ - and  $\omega$ -meson couplings in DD-ME1, are very different from those of the TW-99 effective interaction. The reason is, of course, that only three of these parameters are independent. In our model  $b_\sigma$ ,  $d_\sigma$  and  $d_\omega$  are adjusted to properties of nuclear matter and finite nuclei. Nevertheless, the overall density dependence of the meson-nucleon vertex functions is very similar in the two models, as shown in Fig. 1 for the relevant densities  $\rho \leq 0.3 \text{ fm}^{-3}$ .

Nuclear matter properties calculated with the DD-ME1 interaction are illustrated in Table II and Figs. 2, 3, and 4. The results are shown in comparison with those obtained with the density-dependent effective interaction TW-99 [30], and with two standard non-linear parameter sets NL3 [10] and NL1 [33]. The later non-linear effective interactions have been used extensively in studies of nuclear structure phenomena over the whole periodic table, from light nuclei to superheavy elements. For symmetric nuclear matter all four interactions display similar saturation densities (with NL3 at the low end), and binding energies per nucleon (with NL1 at the high end). While three parameters of TW-99 have been specifically adjusted to the values of  $\rho_{\text{sat}}$ ,  $E/A$  and the incompressibility  $K_0$  shown in Table II, the effective interactions DD-ME1, NL3 and NL1 have been simultaneously

adjusted to properties of nuclear matter and finite nuclei. The incompressibility modulus  $K_0$  of the two density-dependent interactions ( $\approx 240 - 245$ ) MeV lies between the values predicted by the non-linear interactions NL1 and NL3. Calculations of the excitation energies of isoscalar giant monopole resonances in spherical nuclei in the time-dependent relativistic mean-field framework [34], and in the relativistic random-phase approximation [35], suggest that the nuclear matter incompressibility modulus should be in the range  $K_0 \approx 250 - 270$  MeV. All four effective interactions display low values of the effective mass  $m^*$  that are, of course, necessary in order to reproduce the empirical spin-orbit splittings in spherical nuclei. The equations of state of symmetric nuclear matter are compared in Fig. 2. All four binding energy per particle curves display a very similar dependence on density below the saturation point  $\rho_{\text{sat}}$ . Pronounced differences show up at higher densities. In particular, the two non-linear effective interactions NL1 and NL3 display a much steeper increase of the binding energy, especially with respect to TW-99. This is due to the fact that the  $\omega$ -meson, which dominates at higher densities, enters linearly in NL1 and NL3, with constant coupling. The equation of state calculated with the DD-ME1 interaction shows an intermediate density dependence in this region, though closer to NL1 and NL3.

The principal difference between the density-dependent effective interactions DD-ME1 and TW-99 on one hand, and the non-linear interactions NL3 and NL1 on the other, are the properties of asymmetric matter. This is a very important point, because different isovector properties in nuclear matter lead to very different predictions for the properties of exotic nuclei with extreme isospin values. The energy per particle of asymmetric nuclear matter can be expanded about the equilibrium density  $\rho_{\text{sat}}$  in a Taylor series in  $\rho$  and  $\alpha$  [36]

$$E(\rho, \alpha) = E(\rho, 0) + S_2(\rho)\alpha^2 + S_4(\rho)\alpha^4 + \dots \quad (24)$$

where

$$\alpha \equiv \frac{N - Z}{N + Z} . \quad (25)$$

$$E(\rho, 0) = -a_v + \frac{K_0}{18\rho_{\text{sat}}^2} (\rho - \rho_{\text{sat}})^2 + \dots \quad (26)$$

and

$$S_2(\rho) = a_4 + \frac{p_0}{\rho_{\text{sat}}^2} (\rho - \rho_{\text{sat}}) + \frac{\Delta K_0}{18\rho_{\text{sat}}^2} (\rho - \rho_{\text{sat}})^2 + \dots \quad (27)$$

The empirical value at saturation density  $S_2(\rho_{\text{sat}}) = a_4 = 30 \pm 4$  MeV. The parameter  $p_0$  defines the linear density dependence of the symmetry energy, and  $\Delta K_0$  is the correction to the incompressibility. The contribution of the term  $S_4(\rho)\alpha^4$  in (24) is very small in ordinary nuclei and the coefficient is not constrained in the mean-field approximation. We first note that the non-linear effective interactions NL1 and NL3 have a considerably larger value  $a_4$  of the symmetry energy at saturation density. This is also true for other standard non-linear parameter sets, and is due to the fact that the isovector channel of these effective forces is parameterized by a single constant, the density-independent  $\rho$ -meson coupling  $g_\rho$ . With a single parameter in the isovector channel it is not possible to reproduce simultaneously the empirical value of  $a_4$  and the masses of  $N \neq Z$  nuclei. This only becomes possible if a density dependence is included in the  $\rho$ -meson coupling, as it is done in TW-99 and DD-ME1. In a recent analysis of neutron radii in non-relativistic and covariant mean-field models [11], Furnstahl has studied the linear correlation between the neutron skin and the symmetry energy. In particular, he has shown that there is a very strong linear correlation between the neutron skin thickness in  $^{208}\text{Pb}$  and the individual parameters, which determine the symmetry energy  $S_2(\rho)$ :  $a_4$ ,  $p_0$  and  $\Delta K_0$ . The empirical value of  $r_n - r_p$  in  $^{208}\text{Pb}$  ( $0.20 \pm 0.04$  fm from proton scattering data [37], and  $0.19 \pm 0.09$  fm from the alpha scattering excitation of the isovector giant dipole resonance [38]) places the following constraints on the values of the parameters of the symmetry energy:  $a_4 \approx 30 - 34$  MeV,  $2 \text{ MeV}/\text{fm}^3 \leq p_0 \leq 4 \text{ MeV}/\text{fm}^3$ , and  $-200 \text{ MeV} \leq \Delta K_0 \leq -50 \text{ MeV}$ . In Table II we notice that, while these constraints are satisfied by the density-dependent interactions DD-ME1 and TW-99, the parameters of the symmetry energy of the non-linear interactions are systematically much larger. In particular,  $p_0$  is too large by a factor  $\approx 2$ , and the correction to the incompressibility  $\Delta K_0$  has even a wrong sign for the two non-linear interactions. The qualitatively different density dependence of the symmetry energy for the two classes of effective interactions is also illustrated in Fig. 3, where we plot the coefficient  $S_2$  as a function of the baryon density. Due to the very large value of  $p_0$  and the small absolute value of  $\Delta K_0$ , for NL3 and NL1  $S_2$  displays an almost linear density dependence of  $\rho$ . For the two density-dependent interactions, on the other hand, the quadratic term of  $S_2$  dominates, especially at densities  $\rho \geq 0.1 \text{ fm}^{-3}$ .

In Fig. 4 we display the energy per particle of neutron matter as a function of the neutron density. At low densities, which are relevant for nuclear structure problems, the

results for the four relativistic mean-field interactions DD-ME1, TW-99, NL3 and NL1 are shown in comparison with the microscopic many-body neutron matter equation of state of Friedman and Pandharipande [12]. The later is well reproduced by the density-dependent effective interactions, especially by TW-99, while the two non-linear interactions NL3 and NL1 display a qualitatively different neutron matter equation of state, even at very low densities.

The density-dependent effective interaction DD-ME1 has been simultaneously adjusted to nuclear matter properties and to ground-state properties of the spherical nuclei shown in Table III. The calculated binding energies, charge radii and differences between neutron and proton radii are shown in comparison with available experimental data. The choice of the isotopes of Sn and Pb for the fitting procedure was motivated by the desire to construct an effective interaction that could be applied in the description of long isotopic chains, including exotic nuclei which lie very far from the valley of  $\beta$ -stability. The overall agreement between the calculated quantities and experimental data in Table III is very good.

One of the advantages of using the relativistic framework lies in the fact that the effective single-nucleon spin-orbit potential arises naturally from the Dirac-Lorentz structure of the effective Lagrangian. The single-nucleon Hamiltonian does not contain any adjustable parameter for the spin-orbit interaction. In Table IV we compare the energy spacings of spin-orbit partners in the doubly closed-shell nuclei  $^{16}\text{O}$ ,  $^{40}\text{Ca}$ ,  $^{48}\text{Ca}$ ,  $^{132}\text{Sn}$  and  $^{208}\text{Pb}$ , with the values calculated with the DD-ME1 interaction and with the prediction of the standard NL3 non-linear interaction. The experimental data are from Ref. [39]. We notice that, even though the values calculated with NL3 are already in very good agreement with experimental data, a further improvement is obtained with the DD-ME1 interaction, especially for the lighter nuclei  $^{16}\text{O}$ ,  $^{40}\text{Ca}$  and  $^{48}\text{Ca}$ .

#### IV. GROUND STATES OF THE Sn AND Pb ISOTOPES

In Ref. [6] we have applied the relativistic Hartree Bogoliubov (RHB) model in a detailed analysis of ground-state properties of Ni and Sn isotopes. The NL3 parameter set [10] was used for the effective mean-field Lagrangian, and pairing correlations were described by the pairing part of the finite range Gogny interaction D1S [31]. Fully self-consistent RHB solutions were calculated for the isotopic chains of Ni ( $28 \leq N \leq 50$ ) and Sn ( $50 \leq$

$N \leq 82$ ). Binding energies, neutron separation energies, and proton and neutron *rms* radii were compared with experimental data. The reduction of the spin-orbit potential with the increase of the number of neutrons was studied, and the resulting energy spacings between spin-orbit partners were discussed, as well as pairing properties calculated with a finite range effective interaction in the *pp* channel.

In this section we test the new density-dependent meson-exchange effective force DD-ME1 in comparison with the non-linear interaction NL3. The RHB model is used to calculate ground-state properties of Sn and Pb isotopes. Both NL3 and DD-ME1 mean-field Lagrangians are employed for the *ph* channel, and the pairing part of the Gogny interaction D1S is used in the *pp* channel. This pairing interaction is a sum of two Gaussians with finite range and properly chosen spin and isospin dependence. The Gogny force has been very carefully adjusted to the pairing properties of finite nuclei all over the periodic table. Its basic advantage is the finite range, which automatically guarantees a proper cut-off in momentum space. By comparing results of fully self-consistent RHB calculations with experimental data, we will show that the new effective interaction DD-ME1 provides an excellent description of ground-state properties and, as compared with NL3, the isovector channel is considerably improved.

In Fig. 5 we plot the deviations of the theoretical masses of Sn isotopes, calculated in the RHB model with the DD-ME1 and NL3 interactions, from the empirical values [40]. Both interactions display very good results over the entire major shell  $50 \leq N \leq 82$ . For the new interaction DD-ME1, in particular, only in few cases the absolute deviation of the calculated mass exceeds 0.1%.

The isotopic dependence of the difference between the theoretical and experimental charge radii [41] of Sn nuclei is displayed in Fig. 6. The charge radii calculated with both DD-ME1 and NL3 interactions are systematically smaller than the experimental values. The new density-dependent force, however, reduces the deviations from the experimental radii by a factor  $\approx 2$ . The parameters of DD-ME1 have been adjusted to the charge radii of  $^{112,116,124}\text{Sn}$ , and the absolute deviations for these nuclei can be compared in Table III.

The calculated differences between radii of neutron and proton ground-state distributions of Sn nuclei are shown in Fig. 7. The non-linear interaction NL3 systematically predicts larger values of  $r_n - r_p$ . This effect is even more pronounced for the older parameter set NL1 [42]. The difference between the values calculated with NL3 and DD-ME1 increases

with the number of neutrons to about 0.1 fm at  $N = 82$ , but then it remains practically constant for  $N > 82$ . The calculated values of  $r_n - r_p$  are compared with experimental data [43] in Fig. 8. While both interactions reproduce the isotopic trend of the experimental data, NL3 obviously overestimates the neutron skin. The values calculated with DD-ME1, on the other hand, are in excellent agreement with the experimental data. This result presents a strong indication that the isovector channel of the effective interaction DD-ME1 is correctly parameterized.

In Refs. [5, 6] it has been shown that the relativistic mean-field framework predicts a strong reduction of the magnitude of the spin-orbit term in the effective single nucleon potential of nuclei with extreme isospin values. Starting from  $T_z = 0$  nuclei, and increasing the number of neutrons or protons, the effective spin-orbit interaction becomes weaker and this results in a reduction of the energy spacings for spin-orbit partners. The spin-orbit potential originates from the addition of two large fields: the field of the vector mesons (short range repulsion), and the scalar field of the sigma meson (intermediate attraction). In the first order approximation, and assuming spherical symmetry, the spin orbit term can be written as

$$V_{s.o.} = \frac{1}{r} \frac{\partial}{\partial r} V_{ls}(r), \quad (28)$$

where  $V_{ls}$  is the spin-orbit potential

$$V_{ls} = \frac{m}{m_{eff}}(V - S). \quad (29)$$

$V$  and  $S$  denote the repulsive vector and the attractive scalar potentials, respectively.  $m_{eff}$  is the effective mass

$$m_{eff} = m - \frac{1}{2}(V - S). \quad (30)$$

On the neutron-rich side the magnitude of the spin-orbit term  $V_{s.o.}$  decreases as we add more neutrons, i.e. more units of isospin. This is reflected in the energy spacings between the neutron spin-orbit partner states

$$\Delta E_{ls} = E_{n,l,j=l-1/2} - E_{n,l,j=l+1/2}. \quad (31)$$

In Fig. 9 we plot the energy spacings between neutron spin-orbit partners in Sn isotopes, calculated in the RHB model with the DD-ME1 and NL3 effective interactions. The calculated isotopic dependence is almost identical. Both interactions predict a reduction of the energy spacings between spin-orbit partners of  $\approx 50\%$  in the interval  $100 \leq A \leq 150$ .



In order to test the DD-ME1 effective interaction in the region of heavy nuclei, we have calculated the Pb isotopes with  $196 \leq A \leq 214$ . In Fig. 10 we display the deviations of the RHB theoretical masses of Pb isotopes from the empirical values [40]. The accuracy of the binding energies calculated with DD-ME1 is comparable to that obtained with the NL3 interaction. However, in contrast to the case of Sn isotopes, the DD-ME1 interaction systematically gives more binding as compared with NL3, especially for  $A < 208$ .

Due to the intrinsic isospin dependence of the effective single-nucleon spin-orbit potential, the relativistic mean-field models naturally reproduce the anomalous charge isotope shifts [44]. The well known example of the anomalous kink in the isotope shifts of Pb isotopes is shown in Fig. 11. The results of RHB calculations with the DD-ME1 and NL3 effective interactions, and with the Gogny D1S interaction in the pairing channel, are compared with experimental data from Ref. [45]. Both interactions reproduce the general trend of isotope shifts and the kink at  $^{208}\text{Pb}$ . The effect is however, too strong with NL3. The experimental data are better described by the DD-ME1 interaction.

Finally, in Fig. 12 we display the differences between radii of neutron and proton ground-state distributions of Pb isotopes, calculated with the DD-ME1 and NL3 effective interactions. Similar to the case of Sn isotopes, DD-ME1 systematically predicts much smaller values for  $r_n - r_p$ , in better agreement with available experimental data. The experimental values of  $r_n - r_p$  in  $^{208}\text{Pb}$  are:  $0.20 \pm 0.04$  fm deduced from proton scattering data [37], and  $0.19 \pm 0.09$  fm deduced from the alpha scattering excitation of the isovector giant dipole resonance [38]. In a recent analysis of intermediate energy nucleon elastic scattering data, and correlated with analyses of electron scattering data, a value  $\approx 0.17$  fm was suggested for the neutron skin thickness in  $^{208}\text{Pb}$  [46]. As it has been emphasized in a recent analysis of neutron radii in mean-field models [11], the value of  $r_n - r_p$  in  $^{208}\text{Pb}$  is crucial for constraining the isovector channel of effective interactions in the mean-field approach, both in non-relativistic and covariant models.

## V. PARITY-VIOLATING ELASTIC ELECTRON SCATTERING AND NEUTRON DENSITY DISTRIBUTIONS

Data on neutron radii and neutron density distributions provide not only basic nuclear structure information, but they also place additional constraints on effective interactions

used in nuclear models. Potentially, a very accurate experimental method for the determination of neutron densities is the elastic scattering of longitudinally polarized electrons on nuclei. The parity-violating asymmetry parameter, defined as the difference between cross sections for the scattering of right- and left-handed longitudinally polarized electrons, produces direct information on the Fourier transform of the neutron density [47]. A recent extensive analysis of possible parity-violating measurements of neutron densities, their theoretical interpretation, and applications can be found in Refs. [48, 49]

In Ref. [50] we have studied parity-violating elastic electron scattering on ground-state densities of neutron-rich nuclei that were calculated in the RHB model with the NL3 + Gogny D1S interaction. For the elastic scattering of 850 MeV electrons on these nuclei, the parity-violating asymmetry parameters were calculated using a relativistic optical model with inclusion of Coulomb distortion effects. The asymmetry parameters for chains of isotopes were compared, and their relation to the Fourier transforms of neutron densities was studied. In this work we have shown that the new density-dependent effective interaction DD-ME1 predicts ground-state neutron density distributions that are in much better agreement with experimental data. Thus, in this section we include an analysis of parity-violating elastic electron scattering on  $^{208}\text{Pb}$  and on those Sn isotopes for which there are data on  $r_n - r_p$  values.

We consider elastic electron scattering on a spin-zero nucleus, i.e. on the potential

$$\hat{V}(r) = V(r) + \gamma_5 A(r) , \quad (32)$$

where  $V(r)$  is the Coulomb potential, and  $A(r)$  results from the weak neutral current amplitude

$$A(r) = \frac{G_F}{2^{3/2}} \rho_W(r) . \quad (33)$$

The weak charge density is defined

$$\rho_W(r) = \int d^3r' G_E(|\mathbf{r} - \mathbf{r}'|) [-\rho_n(r') + (1 - 4\sin^2\Theta_W)\rho_p(r')] , \quad (34)$$

where  $\rho_n$  and  $\rho_p$  are point neutron and proton densities and the electric form factor of the proton is  $G_E(r) \approx \frac{\Lambda^3}{8\pi} e^{-\Lambda r}$  with  $\Lambda = 4.27 \text{ fm}^{-1}$ ,  $\sin^2\Theta_W = 0.23$  for the Weinberg angle.

In the limit of vanishing electron mass, the electron spinor  $\Psi$  defines the helicity states

$$\Psi_{\pm} = \frac{1}{2}(1 \pm \gamma_5)\Psi , \quad (35)$$

which satisfy the Dirac equation

$$[\boldsymbol{\alpha} \cdot \boldsymbol{p} + V_{\pm}(r)]\Psi_{\pm} = E\Psi_{\pm} , \quad (36)$$

with

$$V_{\pm}(r) = V(r) \pm A(r). \quad (37)$$

The parity-violating asymmetry  $A_l$ , or helicity asymmetry, is defined

$$A_l = \frac{d\sigma_+/d\Omega - d\sigma_-/d\Omega}{d\sigma_+/d\Omega + d\sigma_-/d\Omega} , \quad (38)$$

where  $+$ ( $-$ ) refers to the elastic scattering on the potential  $V_{\pm}(r)$ . This difference arises from the interference of one-photon and  $Z^0$  exchange.

Starting from the relativistic Hartree-Bogoliubov solutions for the self-consistent ground states, the charge and weak densities are calculated by folding the point proton and neutron densities. These densities define the Coulomb and weak potentials in the Dirac equation for the massless electron. The partial wave Dirac equation is solved with the inclusion of Coulomb distortion effects, and the cross sections for positive and negative helicity electron states are calculated. The parity-violating asymmetry parameters are plotted as functions of the scattering angle  $\theta$ , or the momentum transfer  $q$ , and they are compared with the Fourier transforms of the neutron density distributions.

In Fig. 13 we plot the parity-violating asymmetry parameters  $A_l$  for elastic electron scattering from  $^{208}\text{Pb}$  at 850 MeV, as functions of the momentum transfer  $q = 2E\sin\theta/2$ , and compare them with the squares of the Fourier transforms of the neutron densities

$$F(q) = \frac{4\pi}{q} \int dr r^2 j_0(qr) \rho_n(r) . \quad (39)$$

The solid and dotted curves correspond to RHB neutron ground state densities calculated with the NL3 and DD-ME1 effective Lagrangians, respectively. The asymmetries  $A_l$  are of order of  $\leq 10^{-5}$  and increase with the momentum transfer  $q$ . We notice that, even though the values of  $r_n - r_p$  calculated with the two interactions differ by  $\approx 0.07$  fm, the differences between the calculated asymmetry parameters  $A_l$  become more pronounced only for  $q > 1$   $\text{fm}^{-1}$ .

The parity-violating asymmetry parameters  $A_l$  for elastic scattering from even-A isotopes  $^{116-124}\text{Sn}$  at 850 MeV, as functions of the scattering angle  $\theta$ , are shown in Fig. 14. They correspond to the ground-state densities calculated with the DD-ME1 interaction. In

Ref. [50] we have discussed the sensitivity of the asymmetry parameters to the formation of the neutron skin. For the Sn isotopes this effect is illustrated in Fig. 7, where the calculated differences between neutron and proton radii of ground-state distributions are shown in comparison with experimental data. The corresponding asymmetry parameters  $\leq 10^{-5}$  in Fig. 14 display somewhat more pronounced differences between neighboring isotopes only for  $\theta > 15^\circ$ . Finally, in Fig. 15 the calculated asymmetry parameters, as functions of the momentum transfer, are compared with the squares of the Fourier transforms of the neutron densities for  $^{116-124}\text{Sn}$ . Obviously a resolution better than  $\leq 10^{-6}$  for the asymmetry parameters is necessary in order to obtain useful informations on neutron density distributions from parity-violating elastic electron scattering. This resolution might be already available at existing experimental facilities [49]. For the Sn isotopes, in particular, the differences between neighboring isotopes are only seen for  $q \geq 1.5 \text{ fm}^{-1}$ . We should also mention that the magnitude of the calculated asymmetry parameters depends, of course, on the electron energy. For electron energies below 500 MeV the asymmetry parameters are small [50], while above 1 GeV the approximation of elastic scattering on continuous charge and weak densities is not valid any more, and the structure of individual nucleons becomes important.

## VI. SUMMARY AND CONCLUSIONS

In the last couple of years the relativistic Hartree-Bogoliubov (RHB) model has been very successfully applied in the description of a variety of nuclear structure phenomena. With the standard non-linear meson-exchange relativistic mean-field effective interactions in the  $ph$ -channel, however, the predictive power of the RHB model is somewhat limited, especially for isovector properties of exotic nuclei far from  $\beta$ -stability. We have tried to overcome these limitations by extending the RHB model to include density-dependent meson-nucleon couplings. The particular implementation of the model presented in this work is based on the density dependent relativistic hadron field (DDRH) theory [25, 26]. The effective Lagrangian in the  $ph$ -channel is characterized by a density dependence of the  $\sigma$ ,  $\omega$  and  $\rho$  meson-nucleon vertex functions. The single-nucleon Dirac equation includes the additional rearrangement self-energies that result from the variation of the vertex functionals with respect to the baryon field operators, and which are essential for the energy-momentum conservation and the thermodynamical consistency of the model. In this work we have

used the phenomenological density functional forms of the meson-nucleon coupling vertices introduced in the DDRH framework by Typel and Wolter [30]. The parameters of the new effective interaction DD-ME1 have been determined by a multiparameter fit constrained by properties of nuclear matter and by a set of experimental data on ground-state properties of spherical nuclei. Pairing correlations in the  $pp$ -channel of the RHB model are described by the pairing part of the finite range Gogny interaction.

Properties of symmetric and asymmetric nuclear matter calculated with the new density-dependent effective interaction DD-ME1 have been compared to those obtained with the effective interaction of Typel and Wolter [30], and with two standard non-linear parameter sets NL3 [10] and NL1 [33]. It has been shown that the density dependent meson-nucleon couplings improve the behavior of the nuclear matter equation of state at higher densities and reproduce the empirical value of the asymmetry energy at saturation density. The properties of asymmetric nuclear matter are much better described by the two density dependent interactions and, in contrast to the non-linear NL3 and NL1 forces, these interactions reproduce the microscopic many-body neutron matter equation of state of Friedman and Pandharipande.

The RHB model with the density-dependent interaction DD-ME1 in the  $ph$ -channel, and with the finite range Gogny interaction D1S in the  $pp$ -channel, has been tested in the calculation of ground-state properties of Sn and Pb isotopes. Results of fully self-consistent RHB calculations of binding energies, charge radii, differences between neutron and proton radii, spin-orbit splittings, performed with the interaction DD-ME1 and with the non-linear interaction NL3, have been compared with available experimental data. While both interactions predict nuclear masses with the same level of accuracy (absolute deviations  $\approx 0.1 - 0.2\%$ ), the improved isovector properties of DD-ME1 result in a better description of charge radii, and especially the calculated values of  $r_n - r_p$  are in much better agreement with experimental data. The correct description of the data on differences of the radii of neutron and proton ground-state distributions, on neutron radii and neutron density distributions is very important for studies of new phenomena in exotic nuclei far from  $\beta$ -stability (neutron skin, neutron halo, pygmy isovector dipole resonances), for astrophysical applications (properties of neutron stars, neutron capture rates), and for a theoretical interpretation of measurements of parity nonconservation effects in atomic systems (tests of the Standard model of electroweak interactions) [51]. In principle, very accurate data on neutron density distri-

butions could be obtained from the elastic scattering of longitudinally polarized electrons on nuclei. Using the ground-state densities calculated with the DD-ME1 interaction in the RHB model, we have performed an analysis of parity-violating elastic electron scattering on  $^{208}\text{Pb}$  and on those Sn isotopes for which there are experimental data on  $r_n - r_p$ . For the elastic scattering of 850 MeV electrons on these nuclei, the parity-violating asymmetry parameters have been calculated using a relativistic optical model with inclusion of Coulomb distortion effects, and related to the Fourier transforms of the neutron density distributions.

The RHB model with density-dependent meson-nucleon couplings represents a significant improvement in the relativistic mean-field description of the nuclear many-body problem and, in particular, of exotic nuclei far from  $\beta$ -stability. The improved isovector properties of the effective interaction in the  $ph$ -channel on one hand, and the unified description of mean-field and pairing correlations in the Hartree-Bogoliubov framework on the other, offer a unique possibility for accurate studies of nuclei with extreme ground-state isospin values and with Fermi levels close to the particle continuum. Particularly interesting will be studies of deformed nuclei for which unusual shape coexistence phenomena, and even very different proton and neutron ground-state deformations, are expected far from stability and close to the drip-lines. Isovector ground-state deformations could also give rise to exotic modes of low-energy isovector collective excitations. We have already started with density-dependent RHB calculations of deformed nuclei, and work is also in progress on the description of collective excitations in the framework of relativistic RPA/QRPA with density-dependent interactions.

## ACKNOWLEDGMENTS

This work has been supported in part by the Bundesministerium für Bildung und Forschung under project 06 TM 979, and by the Gesellschaft für Schwerionenforschung (GSI) Darmstadt.

=====

- 
- [1] B.D. Serot and J.D. Walecka, Adv. Nucl. Phys. **16**, 1 (1986); Int. J. Mod. Phys. **E6**, 515 (1997).
  - [2] P. Ring, Progr. Part. Nucl. Phys. **37**, 193 (1996).

- [3] W. Pöschl, D. Vretenar, G.A. Lalazissis, and P. Ring, Phys. Rev. Lett. **79**, 3841 (1997).
- [4] G.A. Lalazissis, D. Vretenar, W. Pöschl, and P. Ring, Nucl. Phys. **A632**, 363 (1998).
- [5] G.A. Lalazissis, D. Vretenar, W. Pöschl, and P. Ring, Phys. Lett. **B418**, 7 (1998).
- [6] G.A. Lalazissis, D. Vretenar, and P. Ring, Phys. Rev. C **57**, 2294 (1998).
- [7] D. Vretenar, G.A. Lalazissis, and P. Ring, Phys. Rev. Lett. **82**, 4595 (1997).
- [8] G.A. Lalazissis, D. Vretenar, and P. Ring, Nucl. Phys. **A650**, 133 (1999).
- [9] G.A. Lalazissis, D. Vretenar, and P. Ring, Nucl. Phys. **A679**, 481 (2001).
- [10] G.A. Lalazissis, J. König, and P. Ring, Phys. Rev. C **55**, 540 (1997).
- [11] R.J. Furnstahl, arXiv:nucl-th/0112085.
- [12] B. Friedman and V.R. Pandharipande, Nucl. Phys. **A361**, 502 (1981).
- [13] W. Nazarewicz, Nucl. Phys. **A654**, 195c (1999).
- [14] C.J. Horowitz and J. Piekarewicz, Phys. Rev. Lett. **86**, 5647 (2001).
- [15] C.J. Horowitz and J. Piekarewicz, Phys. Rev. C **64**, 062802 (2001).
- [16] A.R. Bodmer, Nucl. Phys. **A526**, 703 (1991).
- [17] Y. Sugahara and H. Toki, Nucl. Phys. **A579**, 557 (1994).
- [18] M.M. Sharma, A.R. Farhan and S. Mythili, Phys. Rev. **C61**, 054306 (2000).
- [19] J.J. Rusnak and R.J. Furnstahl, Nucl. Phys. **A627**, 495 (1997).
- [20] T. Bürvenich, D.G. Madland, J.A. Maruhn, and P.-G. Reinhard, Phys. Rev. C **65**, 044308 (2002).
- [21] R.J. Furnstahl and B.D. Serot, Nucl. Phys. A **671**, 447 (2000).
- [22] J.L. Friar, D.G. Madland, and B.W. Lynn, Phys. Rev. C **53**, 3085 (1996).
- [23] R.J. Furnstahl, B.D. Serot, and H.-B. Tang, Nucl. Phys. A **615**, 441 (1997).
- [24] R. Brockmann and H. Toki, Phys. Rev. Lett. **68**, 3408 (1992)
- [25] H. Lenske and C. Fuchs, Phys. Lett. **B345**, 355 (1995).
- [26] C. Fuchs, H. Lenske, and H.H. Wolter, Phys. Rev. C **52**, 3043 (1995).
- [27] C.M. Keil, F. Hofmann, and H. Lenske, Phys. Rev. C **61**, 064309 (2000).
- [28] F. Hofmann, C.M. Keil, and H. Lenske, Phys. Rev. C **64**, 025804 (2001).
- [29] F. Hofmann, C.M. Keil, and H. Lenske, Phys. Rev. C **64**, 034314 (2001).
- [30] S. Typel and H.H. Wolter, Nucl. Phys. **A656**, 331 (1999).
- [31] J. F. Berger, M. Girod, and D. Gogny, Nucl. Phys. **A428**, 32 (1984).
- [32] F. de Jong and H. Lenske, Phys. Rev. C **57**, 3099 (1998).

- [33] P.G. Reinhard, M. Rufa, J. Maruhn, W. Greiner, and J. Friedrich; Z. Phys. A **323**, 13 (1986).
- [34] D. Vretenar, G.A. Lalazissis, R. Behnsch, W. Pöschl, and P. Ring, Nucl. Phys. **A621**, 853 (1997).
- [35] Zhong-yu Ma, Nguyen Van Giai, A. Wandelt, D. Vretenar, and P. Ring, Nucl. Phys. **A686**, 173 (2001).
- [36] C.-H. Lee, T.T.S. Kuo, G.Q. Li, and G.E. Brown, Phys. Rev. C **57**, 3488 (1998).
- [37] V.E. Starodubsky and N.M. Hintz, Phys. Rev. C **49**, 2118 (1994).
- [38] A. Krasznahorkay *et al.*, Nucl. Phys. **A567**, 521 (1994).
- [39] NUDAT database, National Nuclear Data Center, <http://www.nndc.bnl.gov/nndc/nudat/>
- [40] G. Audi and A. H. Wapstra, Nucl. Phys. **A595**, 409 (1995).
- [41] E.G. Nadiakov, K.P. Marinova, Yu.P. Gangrsky, At. Data Nucl. Data Tables **56**, 133 (1994).
- [42] M.M Sharma and P. Ring, Phys. Rev. C **45**, 2514 (1992).
- [43] A. Krasznahorkay *et al.*, Phys. Rev. Lett. **82**, 3216 (1999).
- [44] M.M. Sharma, G.A. Lalazissis, and P. Ring, Phys. Lett.B **317**, 9 (1993).
- [45] P. Aufmuth, K. Heilig, and A. Steudel, At. Data Nucl. Data Tables **37**, 462 (1987).
- [46] S. Karataglidis, K. Amos, B. A. Brown, and P. K. Deb, Phys. Rev. C **65**, 044306 (2002).
- [47] T. W. Donnelly, J. Dubach, and Ingo Sick, Nucl. Phys. **A503**, 589 (1989).
- [48] C. J. Horowitz, Phys. Rev. C **57**, 3430 (1998).
- [49] C. J. Horowitz, S. J. Pollock, P. A. Souder, and R. Michaels, Phys. Rev. C **63**, 025501 (2001).
- [50] D. Vretenar, P. Finelli, A. Ventura, G.A. Lalazissis, and P. Ring, Phys. Rev. C **61**, 064307 (2000).
- [51] D. Vretenar, G.A. Lalazissis, and P. Ring, Phys. Rev. C **62**, 045502 (2000).



TABLE I: The effective interaction DD-ME1. The masses and meson-nucleon couplings are shown in comparison with the parameters of the density-dependent mean-field model of Ref. [30] (TW-99).

	DD-ME1	TW-99
$m_\sigma$	549.5255	550.0000
$m_\omega$	783.0000	783.0000
$m_\rho$	763.0000	763.0000
$g_\sigma(\rho_{sat})$	10.4434	10.7285
$g_\omega(\rho_{sat})$	12.8939	13.2902
$g_\rho(\rho_{sat})$	3.8053	3.6610
$a_\sigma$	1.3854	1.3655
$b_\sigma$	0.9781	0.2261
$c_\sigma$	1.5342	0.4097
$d_\sigma$	0.4661	0.9020
$a_\omega$	1.3879	1.4025
$b_\omega$	0.8525	0.1726
$c_\omega$	1.3566	0.3443
$d_\omega$	0.4957	0.9840
$a_\rho$	0.5008	0.515

TABLE II: Nuclear matter properties calculated with the density-dependent effective interactions DD-ME1 and TW-99 [30], and the non-linear parameter sets NL3 [10] and NL1 [33].

	DD-ME1	TW-99	NL3	NL1
$\rho_{sat}$ (fm <sup>-3</sup> )	0.152	0.153	0.149	0.153
E/A (MeV)	-16.20	-16.25	-16.25	-16.42
K <sub>0</sub> (MeV)	244.5	240.0	271.8	211.3
m*	0.578	0.556	0.60	0.57
a <sub>4</sub> (MeV)	33.1	32.5	37.9	43.7
p <sub>0</sub> (MeV/fm <sup>3</sup> )	3.26	3.22	5.92	7.0
$\Delta K_0$ (MeV)	-128.5	-126.5	52.1	67.3

TABLE III: Binding energies, charge radii and differences between neutron and proton radii used to adjust the parameters of the DD-ME1 interaction. The calculated values are compared with experimental data (in parentheses).

	E/A (MeV)	$r_{ch}$ (fm)	$r_n - r_p$ (fm)
$^{16}\text{O}$	-7.974 (-7.976)	2.730 (2.730)	-0.03
$^{40}\text{Ca}$	-8.576 (-8.551)	3.464 (3.485)	-0.05
$^{48}\text{Ca}$	-8.631 (-8.667)	3.482 (3.484)	0.19
$^{90}\text{Zr}$	-8.704 (-8.710)	4.294 (4.272)	0.06
$^{112}\text{Sn}$	-8.501 (-8.514)	4.586 (4.596)	0.11
$^{116}\text{Sn}$	-8.516 (-8.523)	4.616 (4.626)	0.15 (0.12)
$^{124}\text{Sn}$	-8.462 (-8.467)	4.671 (4.674)	0.25 (0.19)
$^{132}\text{Sn}$	-8.352 (-8.355)	4.720	0.27
$^{204}\text{Pb}$	-7.885 (-7.880)	5.500 (5.486)	0.18
$^{208}\text{Pb}$	-7.884 (-7.868)	5.518 (5.505)	0.20 (0.20)
$^{214}\text{Pb}$	-7.764 (-7.772)	5.568 (5.562)	0.27
$^{210}\text{Po}$	-7.857 (-7.834)	5.553	0.18

TABLE IV: Energy separation (in MeV) between spin-orbit partner states in doubly closed-shell nuclei, calculated with the DD-ME1 and NL3 interactions, and compared with experimental data [39].

		DD-ME1	NL3	Exp.
<sup>16</sup> O	$\nu 1p$	6.316	6.482	6.18
	$\pi 1p$	6.249	6.404	6.32
<sup>40</sup> Ca	$\nu 1d$	6.567	6.716	6.00
	$\pi 1d$	6.507	6.630	6.00
<sup>48</sup> Ca	$\nu 1f$	7.689	7.542	8.38
	$\nu 2d$	1.723	0.888	2.02
<sup>132</sup> Sn	$\nu 2d$	1.883	1.573	1.65
	$\pi 1g$	6.244	6.230	6.08
	$\pi 2d$	1.822	1.584	1.75
<sup>208</sup> Pb	$\nu 2f$	2.197	1.860	1.77
	$\nu 1i$	6.839	6.813	5.84
	$\nu 3p$	0.878	0.802	0.90
	$\pi 2d$	1.647	1.525	1.33
	$\pi 1h$	5.837	5.809	5.56

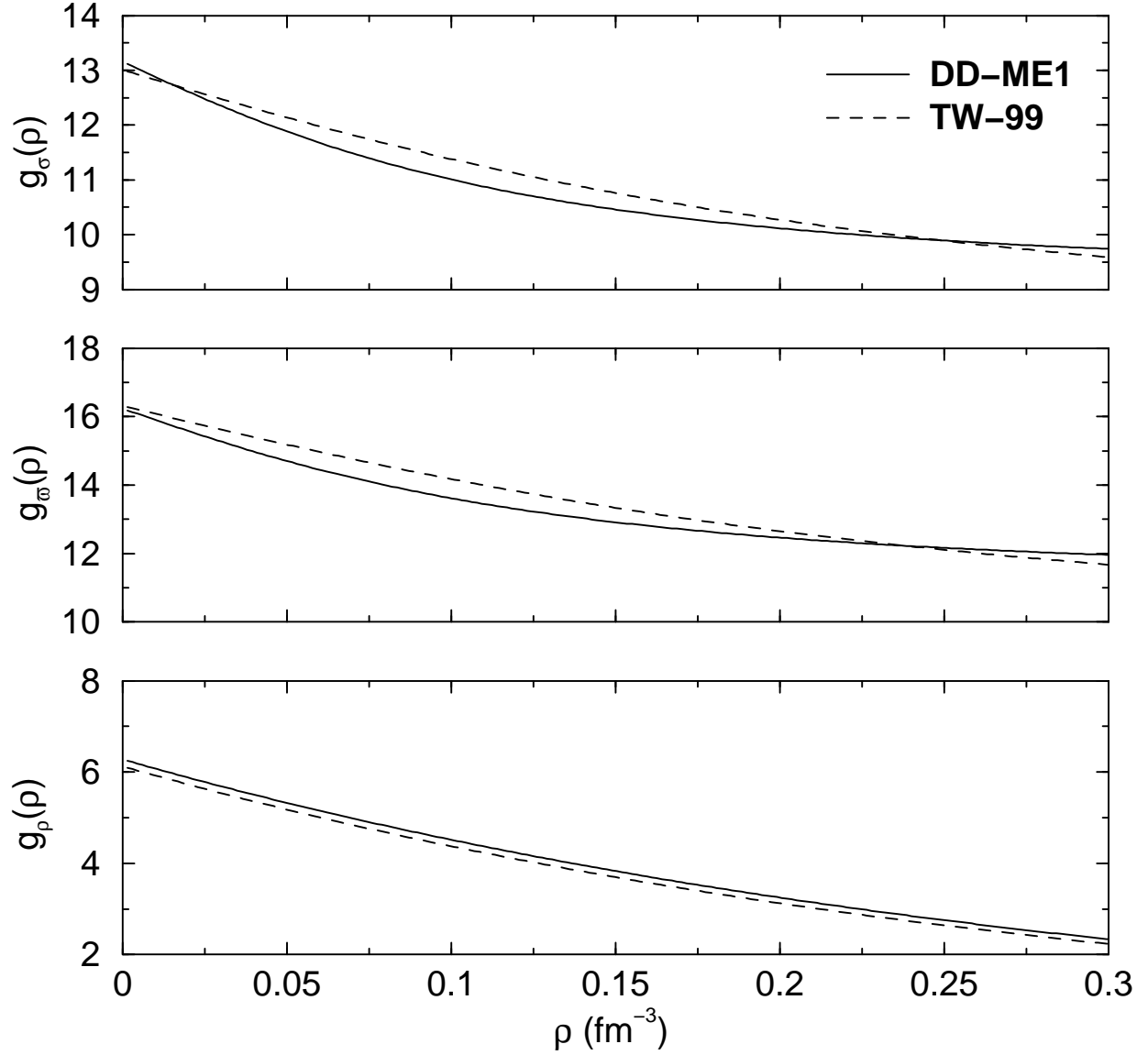


FIG. 1: Density dependence of the couplings of the  $\sigma$ -,  $\omega$ -, and  $\rho$ -meson. The result of the present analysis (DD-ME1) is shown in comparison with the parameters of the effective interaction TW-99 [30].

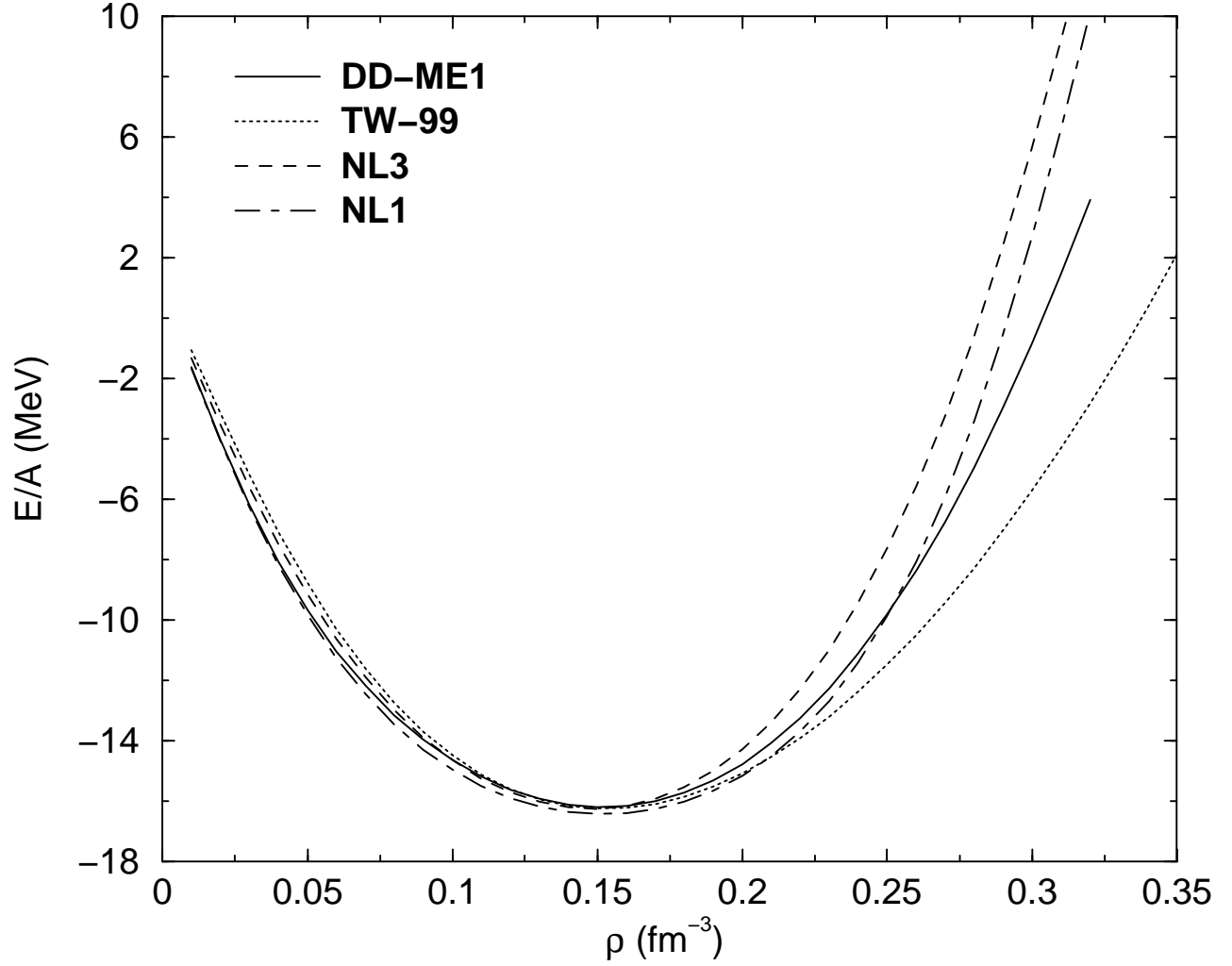


FIG. 2: Binding energy per nucleon for symmetric nuclear matter as a function of the baryon density, calculated with the density-dependent effective interactions DD-ME1 and TW-99 [30], and the non-linear parameter sets NL3 [10] and NL1 [33].

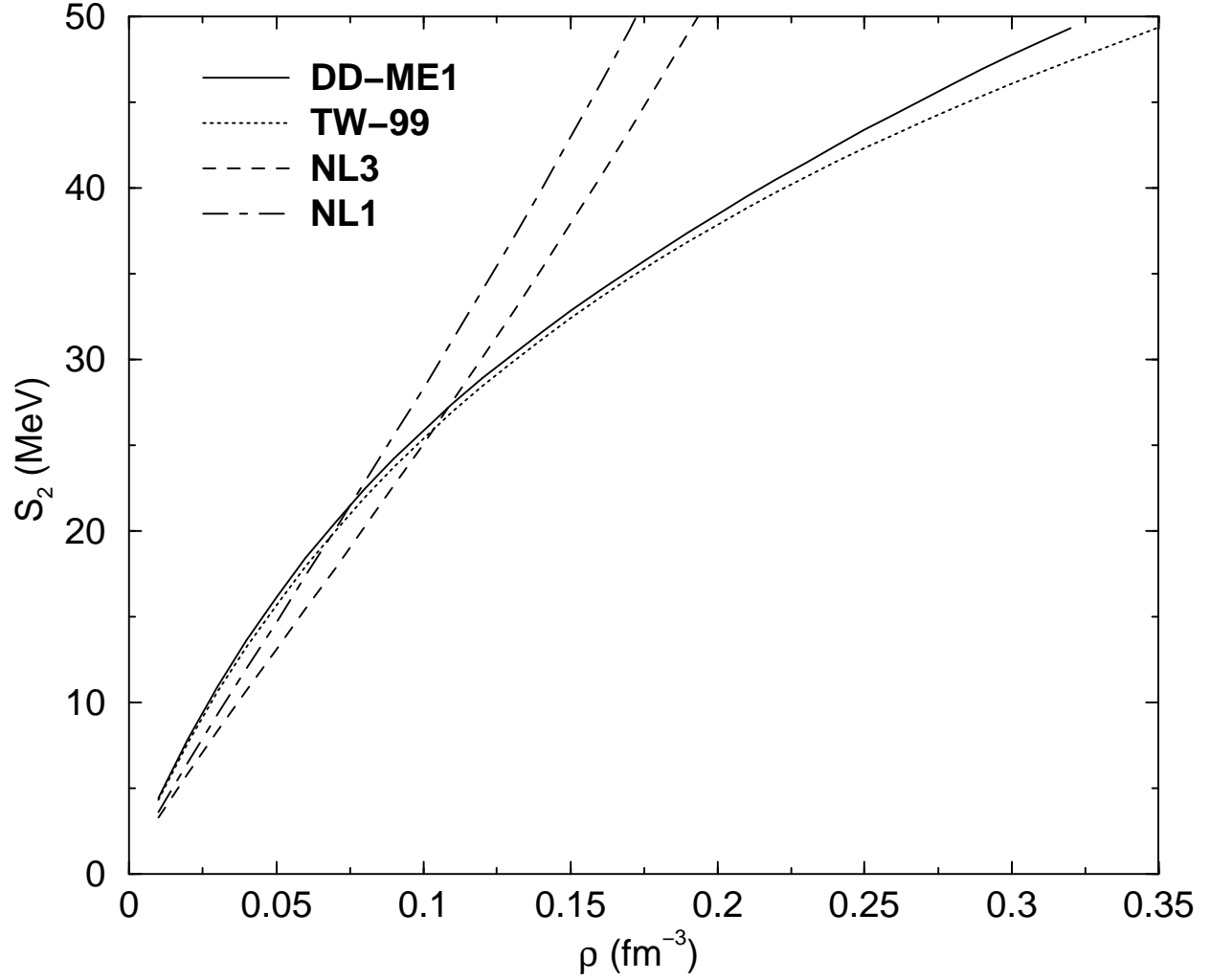


FIG. 3:  $S_2(\rho)$  coefficient (27) of the quadratic term of the energy per particle of asymmetric nuclear matter, calculated with the effective interactions DD-ME1, TW-99 [30], NL3 [10], and NL1 [33].

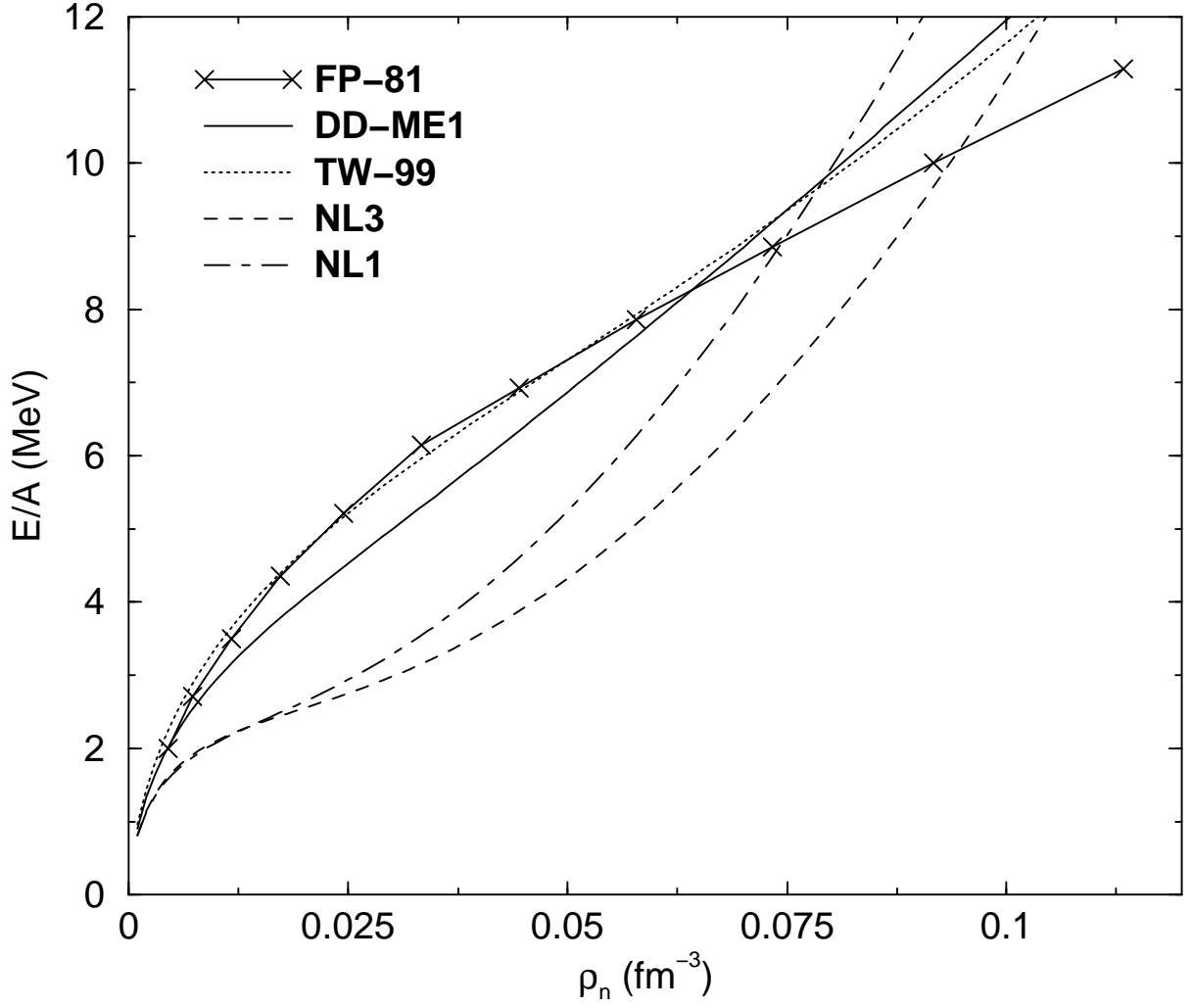


FIG. 4: Energy per particle of neutron matter as a function of the neutron density. The results for the four relativistic mean-field interactions DD-ME1, TW-99 [30], NL3 [10], and NL1 [33] are shown in comparison with the neutron matter equation of state of Friedman and Pandharipande (FP-81) [12].

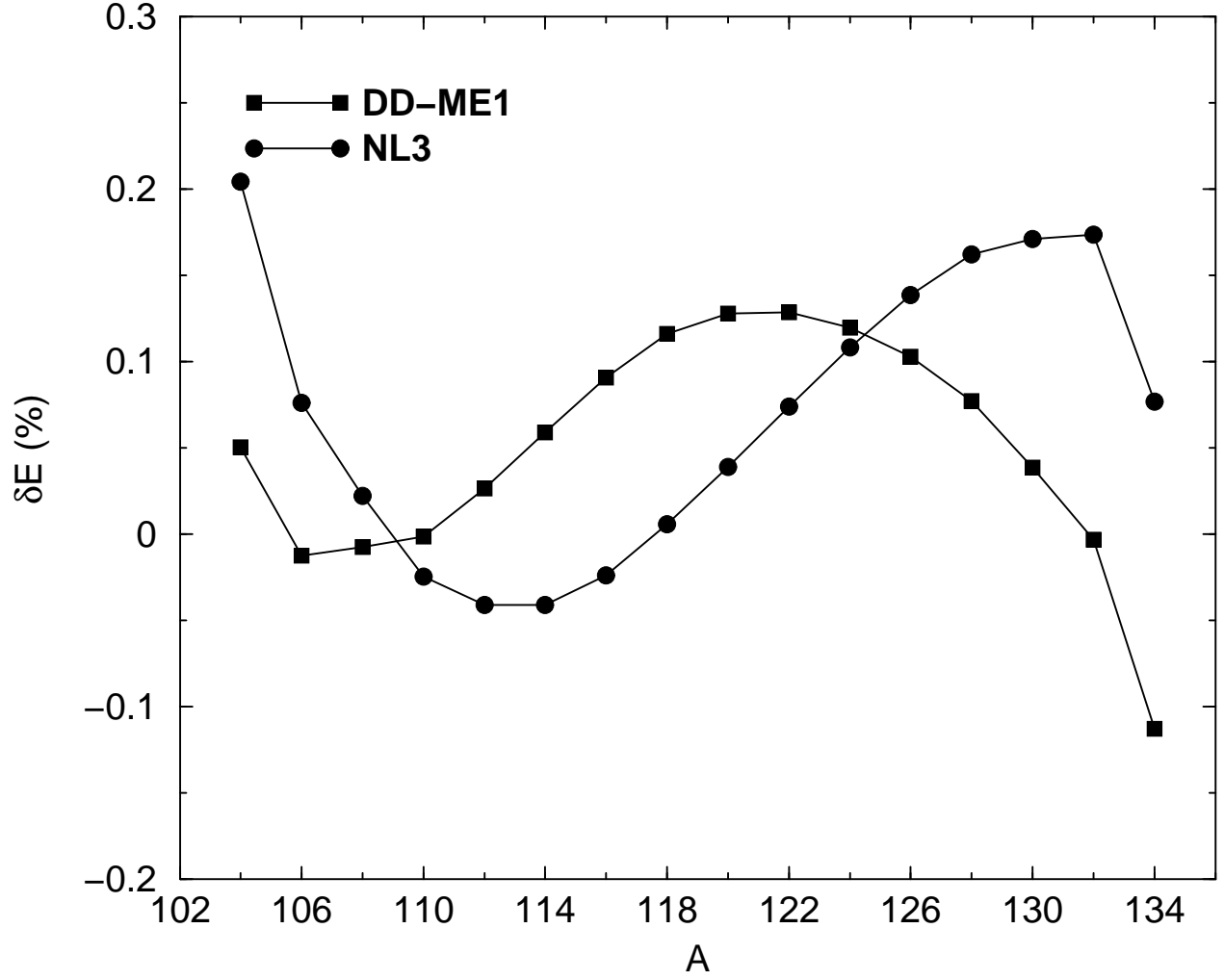


FIG. 5: The deviations (in percent) of the theoretical masses of Sn isotopes, calculated in the RHB model with the DD-ME1 and NL3 interactions, from the empirical values [40]. The pairing part of the Gogny interaction D1S has been used in the  $pp$  channel of the RHB model.



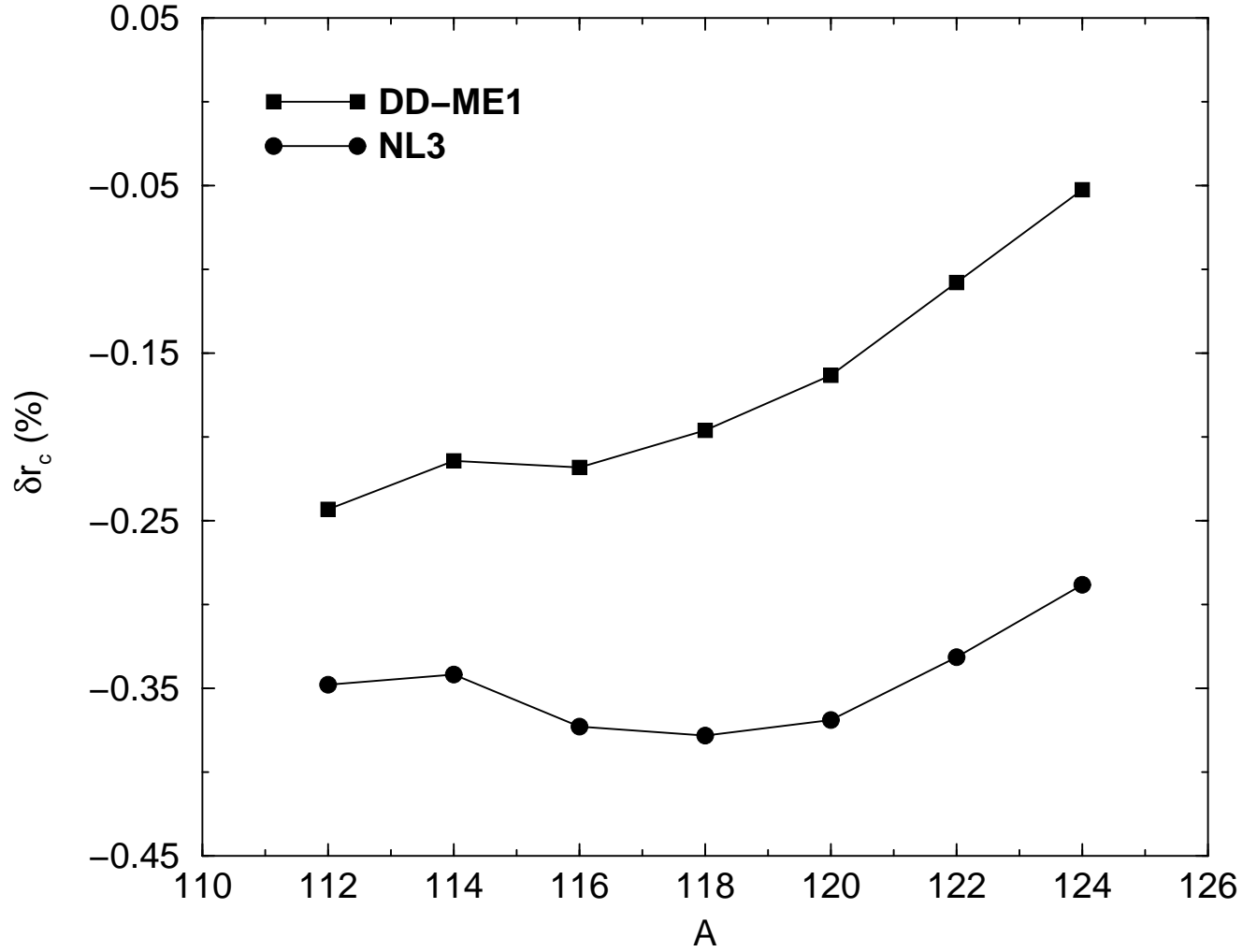


FIG. 6: The deviations (in percent) of the theoretical charge radii of Sn isotopes, calculated in the RHB model with the DD-ME1 and NL3 interactions, from the experimental values [41].

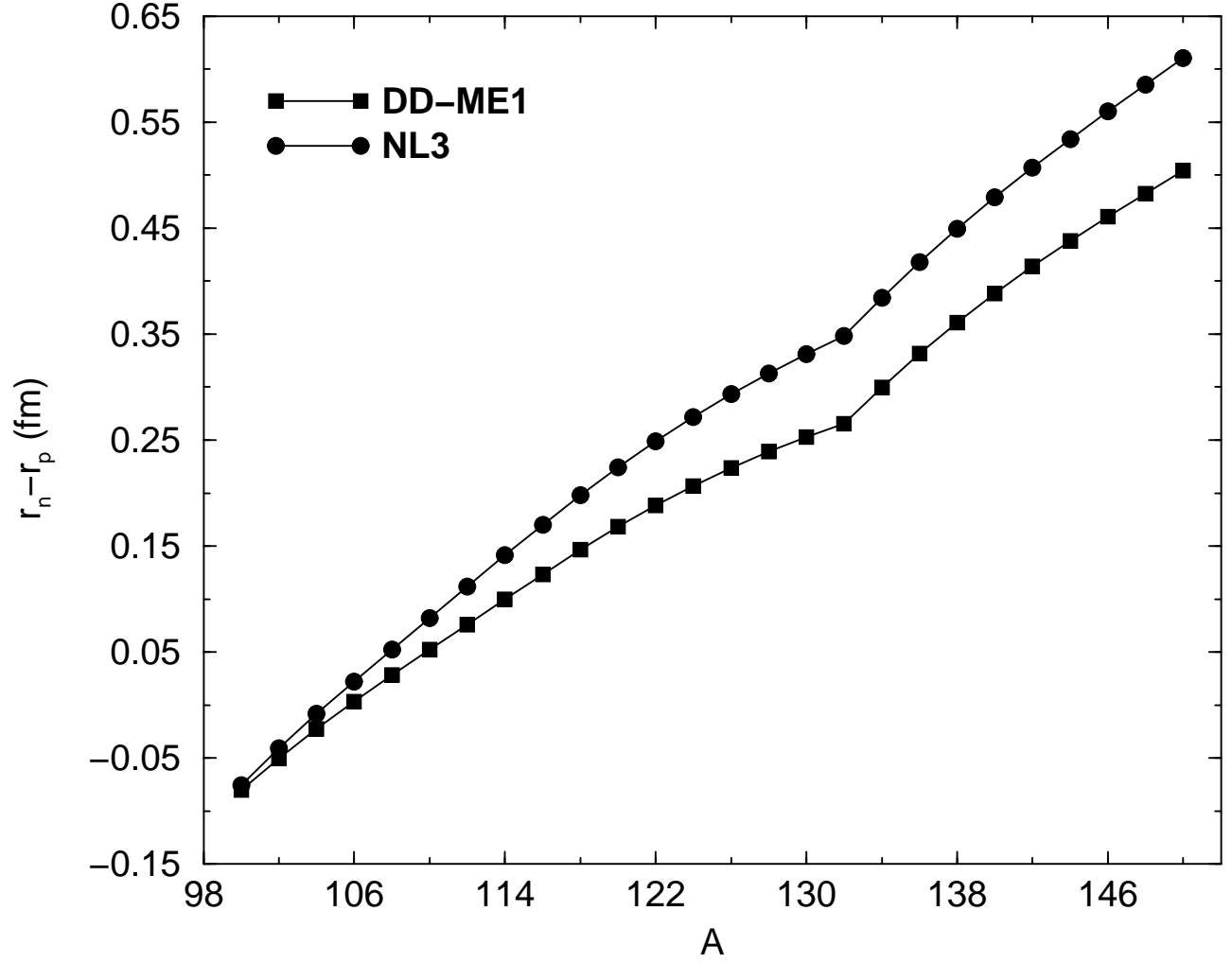


FIG. 7: Differences between neutron and proton radii of ground-state distributions of Sn isotopes, calculated with the DD-ME1 and NL3 effective interactions.

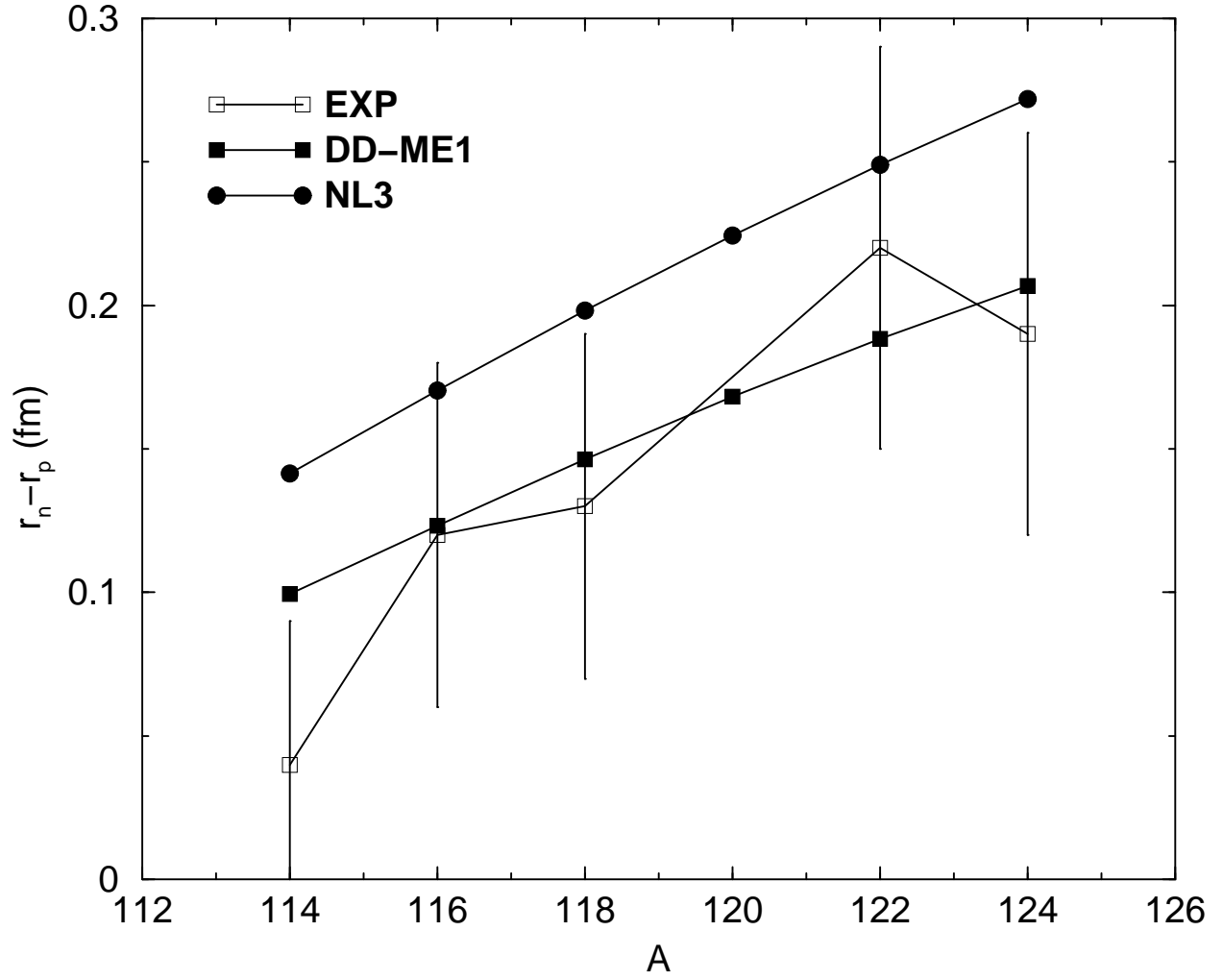


FIG. 8: DD-ME1 and NL3 predictions for the differences between neutron and proton *rms* radii of Sn isotopes, compared with experimental data from Ref. [43].

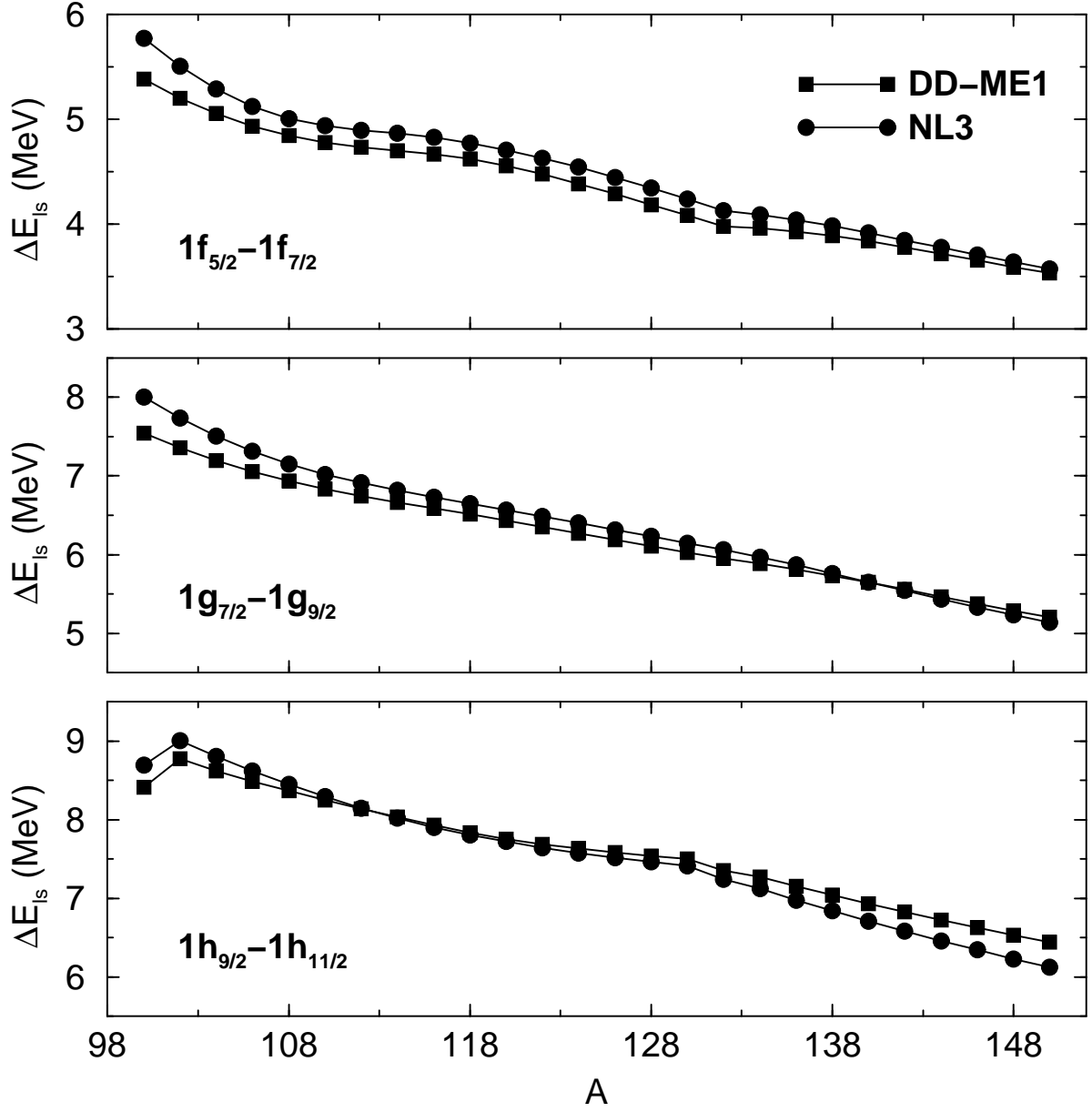


FIG. 9: Energy spacings between neutron spin-orbit partner states in Sn isotopes, calculated in the RHB model with the DD-ME1 and NL3 effective interactions.

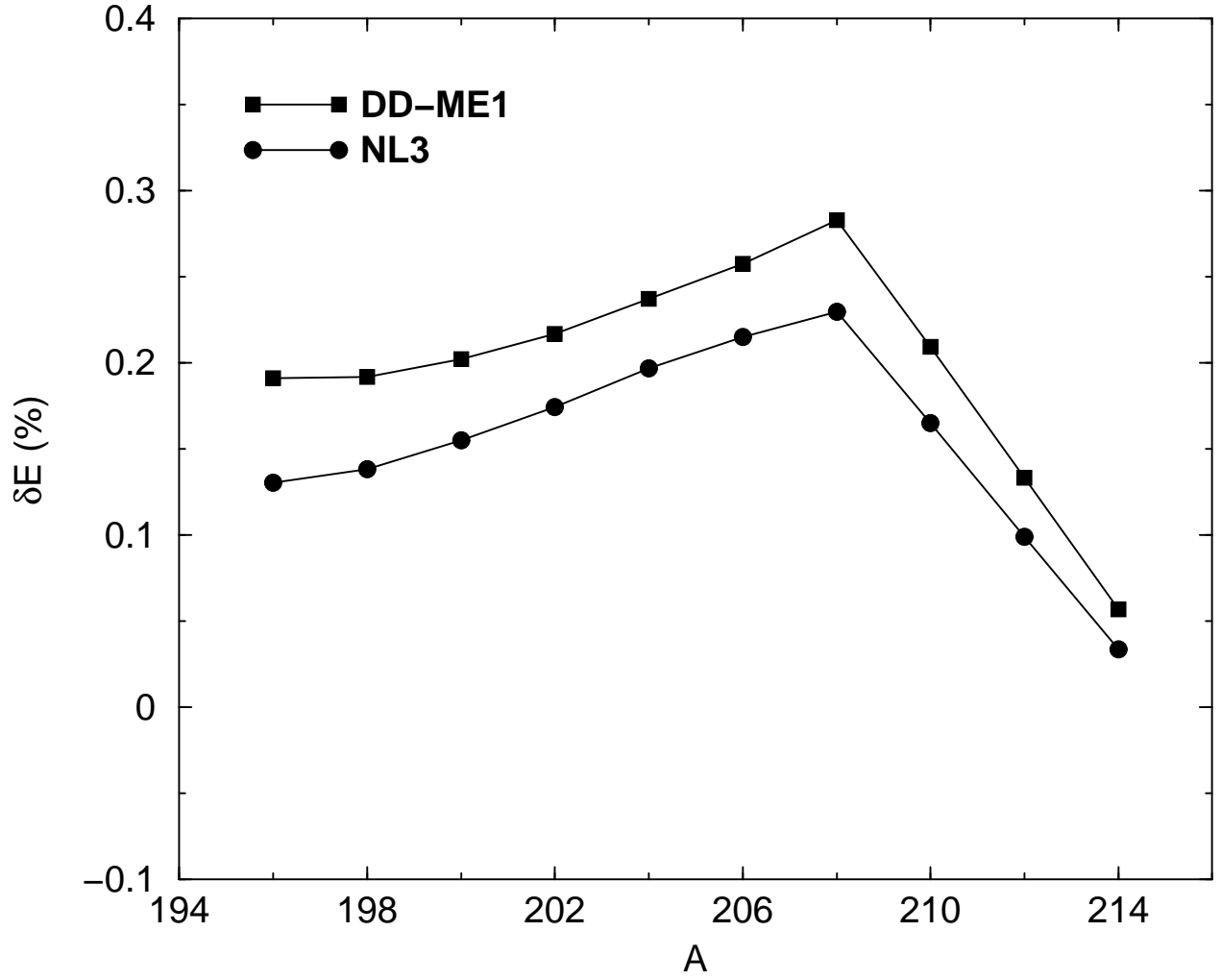


FIG. 10: The deviations (in percent) of the theoretical masses of Pb isotopes, calculated in the RHB model with the DD-ME1 and NL3 interactions, from the empirical values [40].

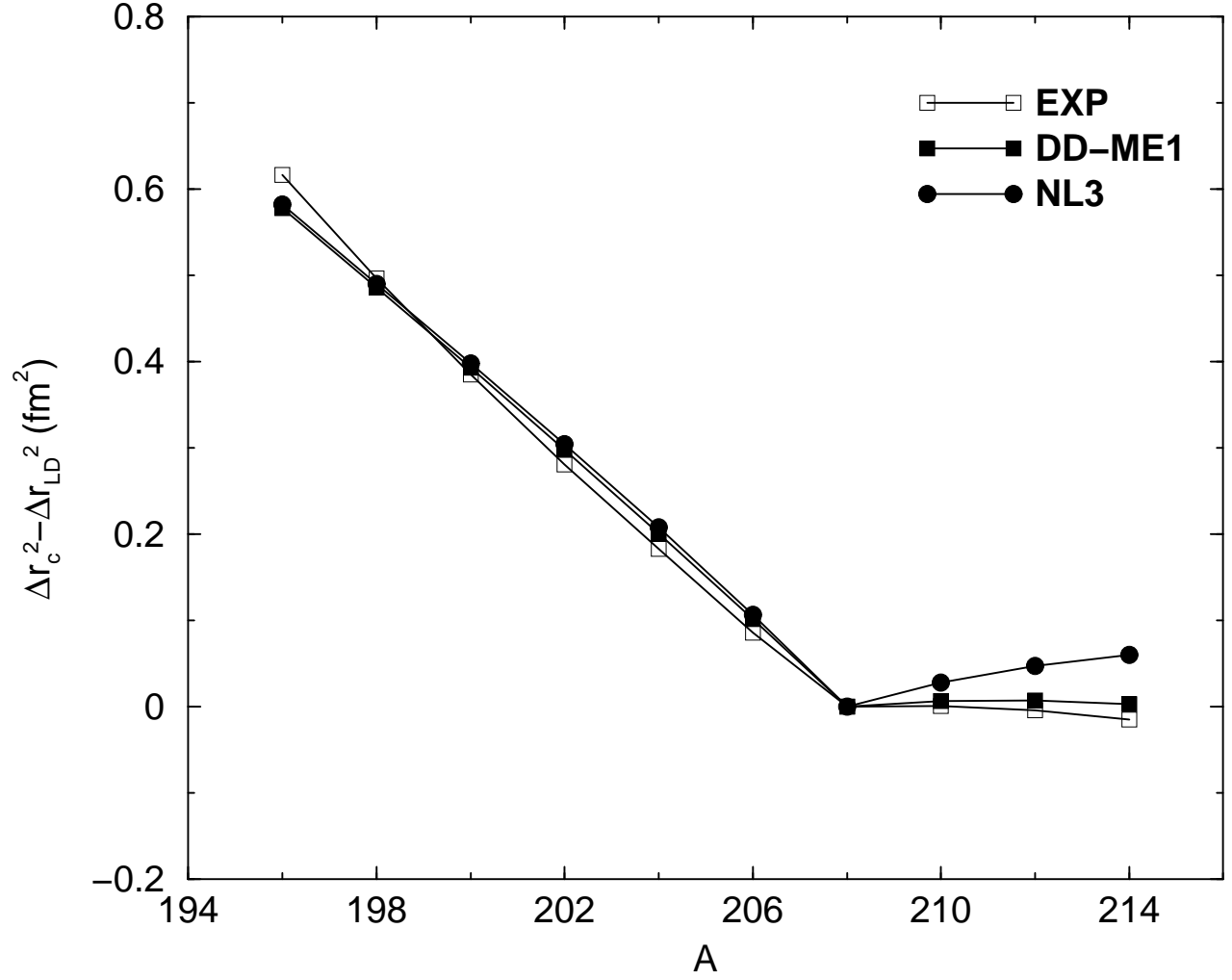


FIG. 11: Charge isotope shifts in even-A Pb isotopes. The results of RHB calculations with the DD-ME1 and NL3 effective interactions, and with the Gogny D1S interaction in the pairing channel, are compared with experimental data from Ref. [45].

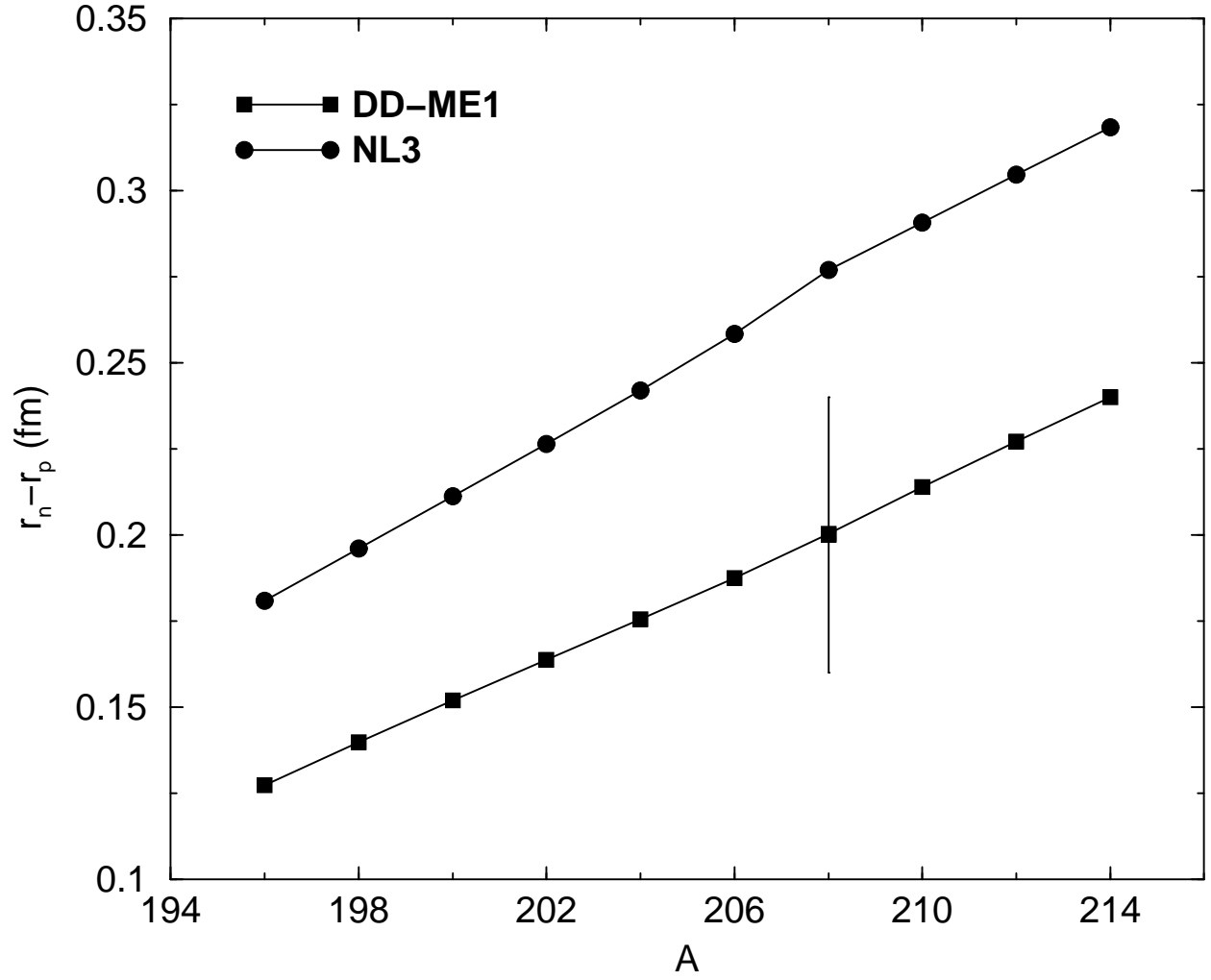


FIG. 12: Differences between neutron and proton radii of ground-state distributions of Pb isotopes, calculated with the DD-ME1 and NL3 effective interactions.

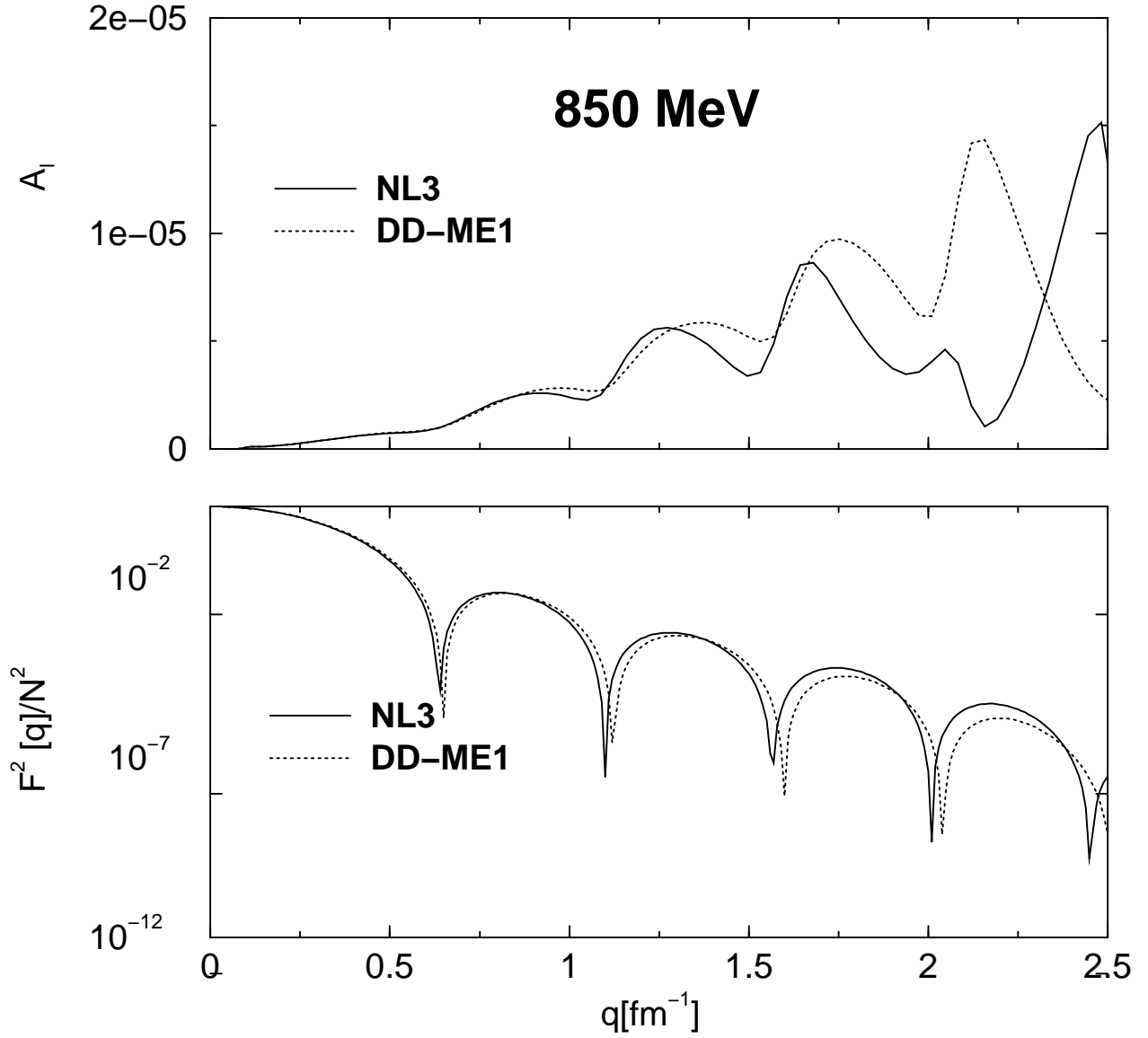


FIG. 13: Parity-violating asymmetry parameters  $A_l$  (upper panel) and squares of normalized Fourier transforms of neutron densities (lower panel), as functions of the momentum transfer  $q$ , for elastic scattering from  $^{208}\text{Pb}$  at 850 MeV.



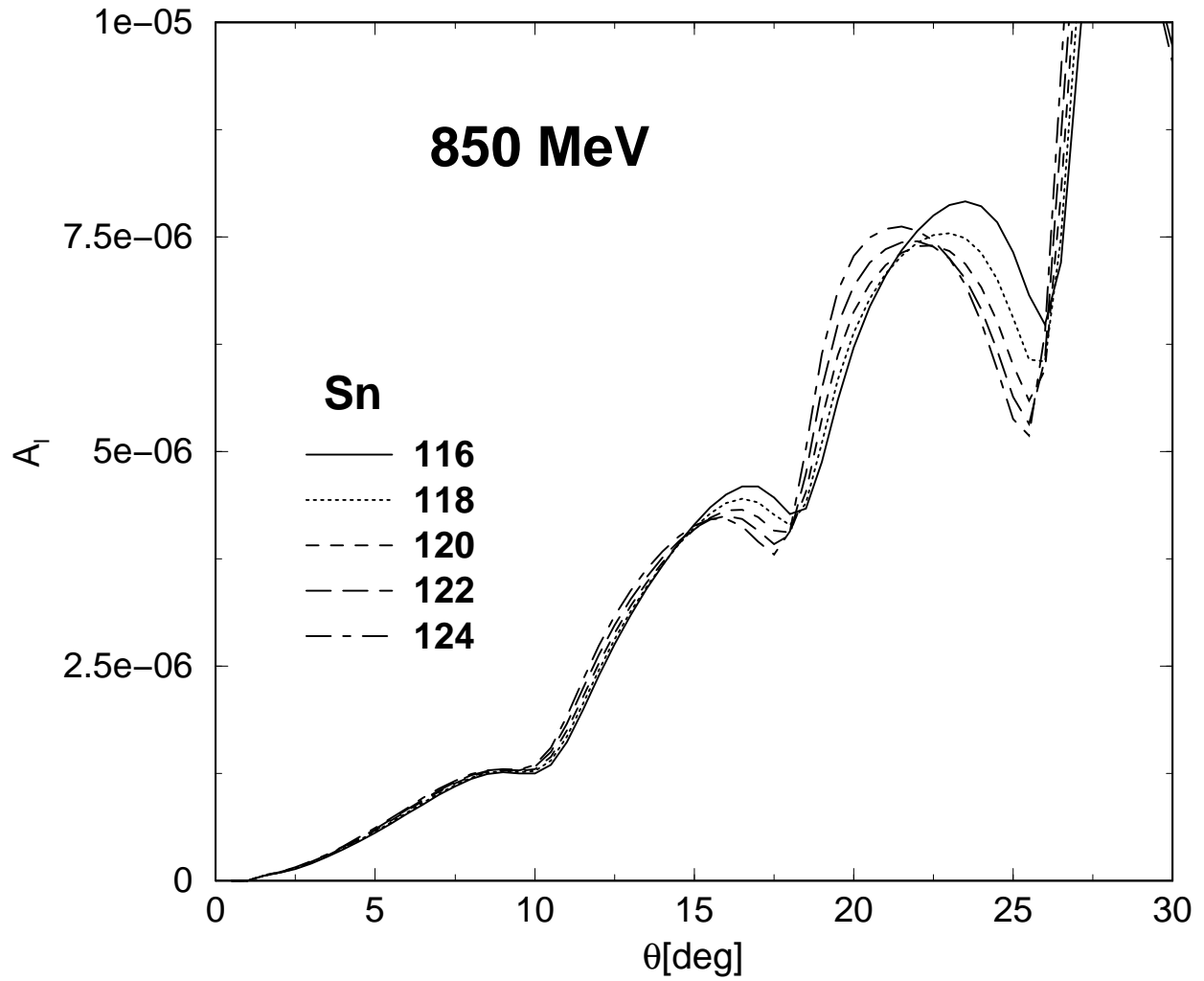


FIG. 14: Parity-violating asymmetry parameters  $A_l$  for elastic scattering from  $^{116-124}\text{Sn}$  at 850 MeV, as functions of the scattering angle  $\theta$ .

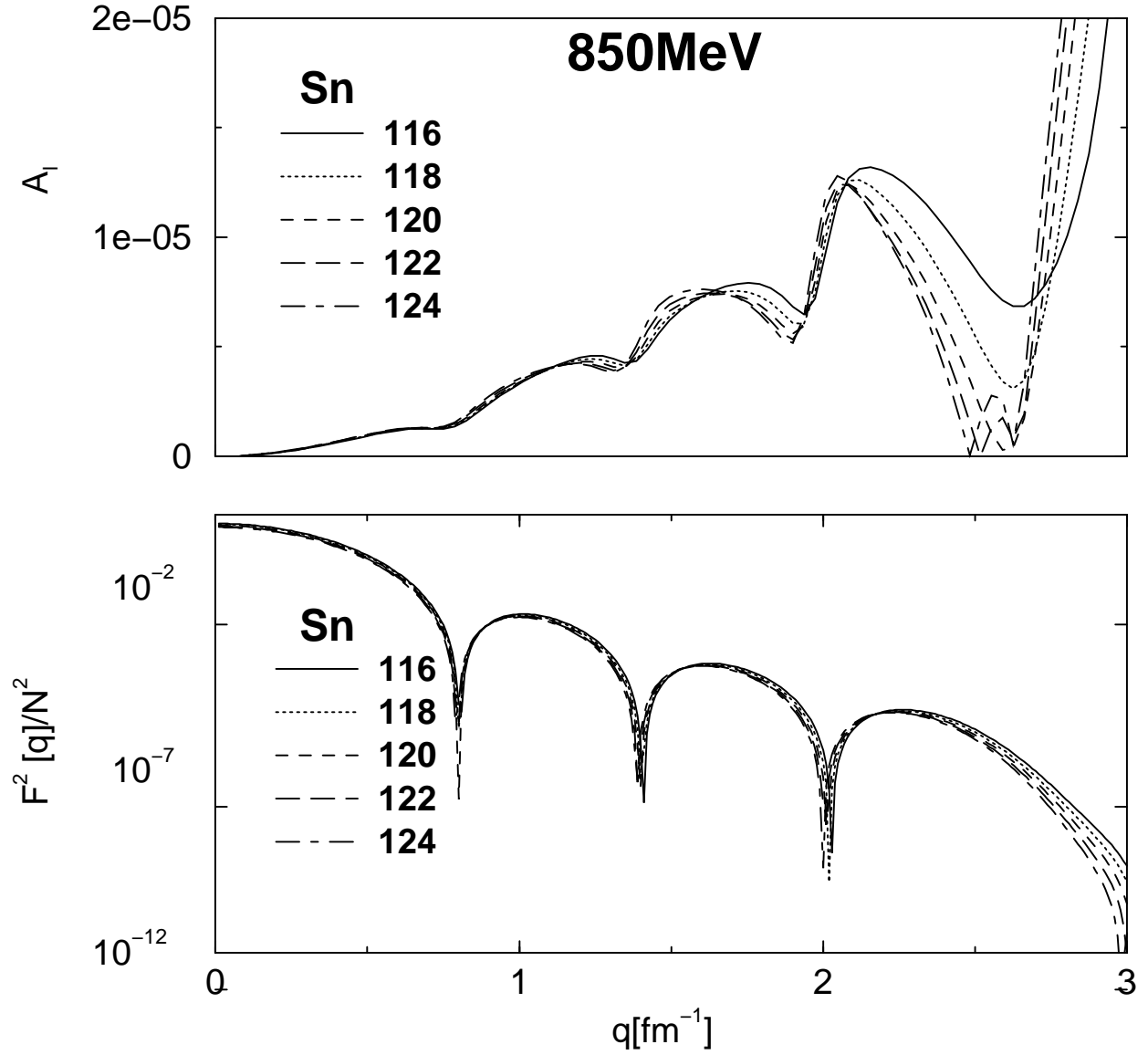


FIG. 15: Parity-violating asymmetry parameters  $A_l$  (upper panel) and squares of normalized Fourier transforms of neutron densities (lower panel), as functions of the momentum transfer  $q$ , for elastic scattering from  $^{116-124}\text{Sn}$  at 850 MeV.